Characterization of the Carbonate System across the Agulhas and Agulhas Return Currents.

Prepared by:

Lebohang Innocentia Melato

MLTLEB004

Prepared for:

Dr. Isabelle J. Ansorge and Dr. Pedro M.S. Monteiro

October 2014

Submitted to the Department of Oceanography at the University of Cape Town in partial fulfilment of the academic requirements for MSc degree in Ocean and Climate Dynamics.

Abstract

In this study, we investigate the role that the solubility and biological pumps have on CO_2 variability across the Agulhas Current system (Agulhas Current and the Agulhas Return Current). The Agulhas Current system transports heat and salt from the Indian Ocean into the South Atlantic Ocean via the Agulhas leakage, which influences the Atlantic Meridional Overturning Circulation (AMOC). This study presents for the first time a characterization of the role the Agulhas Current system (Agulhas and Agulhas Return Currents) has on the uptake of anthropogenic CO_2.

Fugacity of carbon dioxide (fCO_2) values were obtained from a ship-based underway pCO_2 (partial pressure of carbon dioxide) system and the air-sea CO_2 fluxes were computed using 6-hourly wind speeds from the NOAA Blended Sea Winds. An experiment was conducted during the Crossroads scientific monitoring line in May 2013, where surface dissolved inorganic carbon, total alkalinity and CO_2 flux were compared between the Agulhas and Agulhas Return Currents and the region directly south over the Agulhas Plateau.

Our findings highlighted that the solubility and biological pumps played minimal to no role in the drawdown of carbon across the sub-Tropical zone and the Agulhas Current system (Agulhas and Agulhas Return Currents), due to opposing effect between chlorophyll and temperature on pCO_2 that explained why although there was carbon drawdown by primary production in the Agulhas and Agulhas Return Current regions, this does not play a role in enhancing the air – sea exchange of CO_2. The solubility pump was responsible for CO_2 in the sub-Antarctic zone.

The biological and solubility pumps were responsible for CO_2 sink in the Agulhas Plateau eddy. The highest CO_2 flux in the study was observed in the Agulhas Plateau eddy at a flux value of -8.12 $mmolC.m^{-2}.day^{-1}$ due to the cooler mean sea surface temperature of ~16.5 °C.

This is the first time that such as study has been undertaken and aims to provide a better understanding of the role of Western Boundary Currents such as the Agulhas Current has in the uptake of CO_2.

Acknowledgements

I am extremely grateful to have had Dr Isabelle Ansorge and Dr Pedro Monteiro as my supervisors. Their constant support, knowledge and guidance made this thesis an enjoyable yet challenging project.

This research was supported and funded by the South African Department of Environmental Affairs Antarctic Support and Logistics (DEA) and the Department of Science and Technology and National Research Foundation through their SANAP programme.

Many thanks to Warren Joubert and Luke Gregor for their great CO_2 advice. Most importantly I'd like to thank Charine Collins for her assistance in the analysis of satellite data using Matlab and Mutshutshu Tsanwani (DEA) for assisting me with all the CO_2 data collected in 2013.

Table of Contents

1. Introduction

1.1 The Agulhas Current system and ocean circulation

1.1.1 Agulhas Current

The Agulhas Current forms near southern Mozambique (Lutjeharms, 2006) with water masses originating from three independent sources: the Mozambique Channel (Saetre and da Silva, 1984), the East Madagascar Current (also a WBC) (Lutjeharms et al, 1981) and the South West Indian Ocean sub-gyre (by far the largest water mass contributor) (Stramma et al, 1990). The Agulhas Current flows along the continental shelf boundary of southeast Africa (Figure 1.1), from ~27 - 40 °S (Grüindlingh, 1983) until it reaches the southern tip of Africa where it retroflects allowing its water to flow into the Atlantic and Indian Ocean basins. The current has a flow velocity >2 $m.s^{-1}$ and extends >2500 m (Lutjeharms, 2006). The Agulhas Current is supplied with Indian Ocean Tropical Surface Water and Tropical Thermocline Water (Lutjeharms and Ansorge, 2001) of low salinity (34.8 – 35.1) from the Tropics (Gordon et al, 1987) and the more saline (>35.4) South Indian sub-Tropical Surface Water from the South West-Indian Ocean sub-gyre (Wyrtki, 1971). The volume transport of the Agulhas Current at 32 °S was estimated by Bryden et al (2005) to be 70 Sv (1Sv = 10^6 m^3 s^{-1}). This current feeds into the Agulhas Retroflection south of Africa, where approximately 20 – 30% of the water enters the Atlantic Ocean as the Agulhas leakage while the remainder re-circulates into the Indian Ocean as the Agulhas Return Current (Lutjeharms and Ansorge, 2001; van Sebille et al, 2010; Beal and Biastoch, 2010). The region between 35 - 40 °S in the south-western Indian Ocean represents a transitional zone bordered by the Agulhas Return Current and the sub-Tropical Front (e.g., Lutjeharms and van Ballegooyen, 1984; Belkin and Gordon, 1996). This region separates the oligotrophic warm waters of the subtropics from the more productive waters of the sub-Antarctic zone (Metzl, 2009) (Figure 1.1).

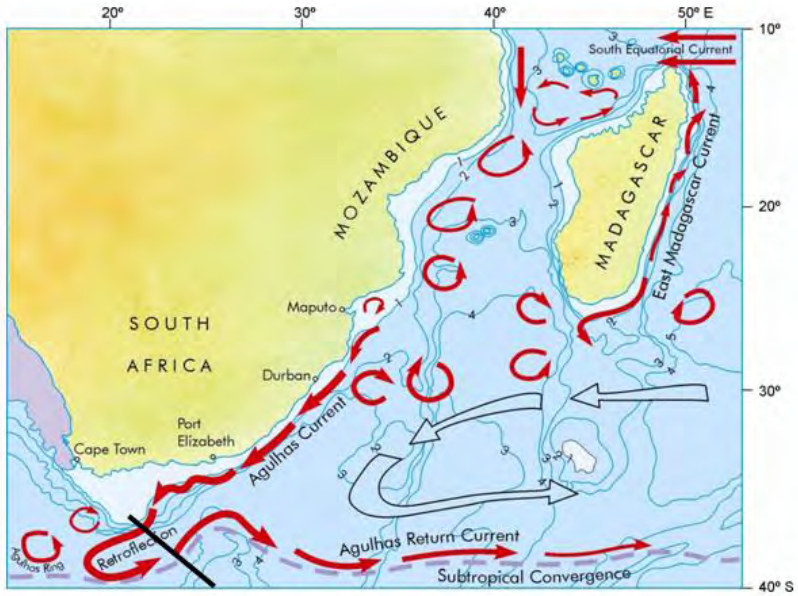

Figure 1.1: A simplified representation of the circulation and currents of the Agulhas Current system. A curved red arrow denotes anticyclonic and cyclonic motions or eddies, and a broken, pink line gives the average location of the sub-Tropical Convergence. Open arrows denote inferred general motion of the Southwest Indian subgyre. Depth is given in kilometre. All the generic components of the current system are shown, including the source currents of the Agulhas Current, its outflows as well as the northern and southern Agulhas Current themselves, located to either side of Port Elizabeth (after Ansorge and Lutjeharms, 2007). The black line refers to the location of the Crossroads transect.

Water masses entering the Agulhas Current system can exit via two major pathways. The first pathway flows eastwards into the South Indian Ocean as the Agulhas Return Current along the boundary of the sub-Tropical Front (STF), while the second pathway flows westwards as a series of Agulhas Rings into the Atlantic Ocean and more commonly known as the Agulhas leakage (van Sebille et al, 2010). The Agulhas Rings are not part of this study as we are focusing on Agulhas Current, Agulhas Return Current and an eddy over the Agulhas Plateau; thus the second pathway will not be included in this study.

1.1.2 Pathway 1- Agulhas Return Current

Emerging from the Agulhas Retroflection (Figure 1.1) the Agulhas Return Current is located ~ at 39°30′ S and extends as far south as 44°30′ S (Lutjeharms and Ansorge, 2001). The trajectory of this current was determined first from drifting bouys (Hoffman, 1985) confirming that its general motion is zonal with extensive meridional deviations, which

correlate to the bathymetry encountered along its path (Darbyshire, 1972; Lutjeharms and van Ballegooyen, 1984). The Agulhas Plateau lies directly within the path of the Agulhas Return Current and thus acts as a major bathymetric obstacle resulting in meanders and mesoscale eddies occurring over the 400 km long plateau. The region is one of extreme mesoscale variability (Cheney et al, 1983) because of recurrent eddy generation (Lutjeharms, 1988) but also shifts causing time-varying meanders in the path of the Agulhas Return Current along the sub-Tropical Front (Lutjeharms and Ansorge, 2001).

The Agulhas Return Current exhibits eastward surface velocities of ~2 ms^{-1} (Lutjeharms and Valentine, 1984) and a volume transport of ~54 Sv (Lutjeharms and Ansorge, 2001). The current extends as far east as ~ 72 °E (Park et al, 1991; Park et al, 1993). Belkin and Gordon (1996) observed water masses of the Agulhas Current origin close to the South-east Indian Ridge at 78 °E, indicative of its eastward extent. According to Mey and Walker (1990), the mean heat loss across this current is ~200 $W.m^{-2}$, consequently evaporation exceeds precipitation, because of changing temperature/salinity characteristics of the upper layers in the retroflection region.

1.2 The Agulhas Current as a potential CO_2 sink

The Agulhas Current is primarily driven by the large-scale pattern of wind stress curl between the southeast trade winds and the Southern Hemisphere westerlies (Beal et al, 2011). According to Rouault et al (2009), high evaporation rates, vital turbulent latent and sensible heat fluxes are a result of the sea surface temperature contrasts between western boundary currents (WBCs) and their surroundings, causing a significant transfer of energy between the surface and the atmosphere (Yu, 2007). Furthermore, Rouault et al (2003) confirmed that the climatologically heat fluxes associated with the Agulhas Current are smaller than those for the Gulf Stream and the Kuroshio Currents (also WBCs), since the marine air masses that are advected by the westerlies over the southern Agulhas Current are typically less cold and dry than those transported over the Gulf Stream and the Kuroshio Currents. In addition, winter latent and sensible fluxes over the Agulhas Current range between 100 – 150 Wm^{-2} and 15 – 30 Wm^{-2} respectively (Josey et al, 1999). There is generally less seasonal variability in the Agulhas Current system, heat losses to the atmosphere and consequently the Agulhas Current system drives oceanic uptake of anthropogenic carbon dioxide (CO_2). Sabine et al (2004) estimated that 48% of fossil fuel CO_2 resides in the ocean with the Atlantic Ocean alone

contributing 38% to the anthropogenic oceanic carbon storage, even though it only represents 29% of the global ocean surface area.

According to Beal et al (2011), Agulhas rings could influence atmospheric CO_2 concentrations by injecting warm and salty waters into the South Atlantic. Furthermore, Rouault et al (2009) confirmed that the temperature of the Agulhas Current system (Figure 1.1) has increased by up to 0.7 °C per decade since the 1980's, suggesting that the Agulhas Leakage is warming. This increased warming may reduce the ability of the ocean south of Africa to absorb CO_2. Thus, the aim of this study is to investigate the role of the Agulhas Current system as a CO_2 sink using data collected along the first Crossroads transect in May 2013.

2. Literature Review

2.1 An overview of the carbon dioxide global system

The anthropogenic accumulation of atmospheric carbon dioxide (CO_2), a product of burning fossil fuels, dates back to the fossil fuel era in 1751 (Andres et al, 1999). Since the industrial revolution (1760 - 1840), anthropogenic CO_2 emissions increased dramatically from ~5.5 PgC/yr (1Pg = 10^{15} g) in 1970, to ~8.4 PgC/yr in 2000 (Raupach et al, 2007) and rising to 9.9 PgC/yr in 2006 (Canadell et al, 2007; Metzl, 2009). With the rapid consumption of fossil fuels, atmospheric CO_2 is predicted to increase further, between 700 and 1000 ppm by the end of the century (IPCC, 2001; Caldeira and Wickett, 2003). A side effect of this increase in atmospheric CO_2 is a decrease in sea surface water pH levels of ~0.4 by 2100, and a corresponding 50% decrease in carbonate ion concentration (Caldeira and Wickett, 2003). Furthermore, changes in pH levels and carbonate ion concentration negatively affect the community structure and distribution of fragile marine species, such as coccolithophores.

The ocean plays a fundamental role in modulating the exchange of atmospheric CO_2 through a variety of physical, chemical and biological processes. From 1800 to 1994 the ocean has consumed ~50% of the total anthropogenic CO_2 emissions, thus substantially moderating global warming (Sabine et al, 2004). Without this uptake, the Earth's anthropogenic CO_2 levels would have exceeded 450 μatm, which corresponds with the maximum atmospheric CO_2 level allowed to keep global warming below the 2˚C threshold (IPCC, 2007). Currently, the global ocean is a sink for atmospheric CO_2 with uptake rates estimated between 1.4 and 2.3 $PgCy^{-1}$ ($Pg=10^{15}gC$; Le Quéré et al, 2009; Takahashi et al, 2009), approximately 15 – 26% of the anthropogenic CO_2 emissions (Andersson et al, 2013).

Carbon uptake by the ocean is controlled by two important mechanisms: the solubility (physical) pump and the biological pump (Figure 2.1) (Takamitsu and Follows, 2003). The solubility pump reflects how the solubility of CO_2 is dependent on water temperature, hence cold waters are generally more enriched in dissolved inorganic carbon, due to their higher solubility coefficient, than warmer waters (Takamitsu and Follows, 2003). The biological

pump refers to processes that are responsible for the draw-down of approximately three-quarters of the dissolved inorganic carbon from the surface to the deep-ocean.

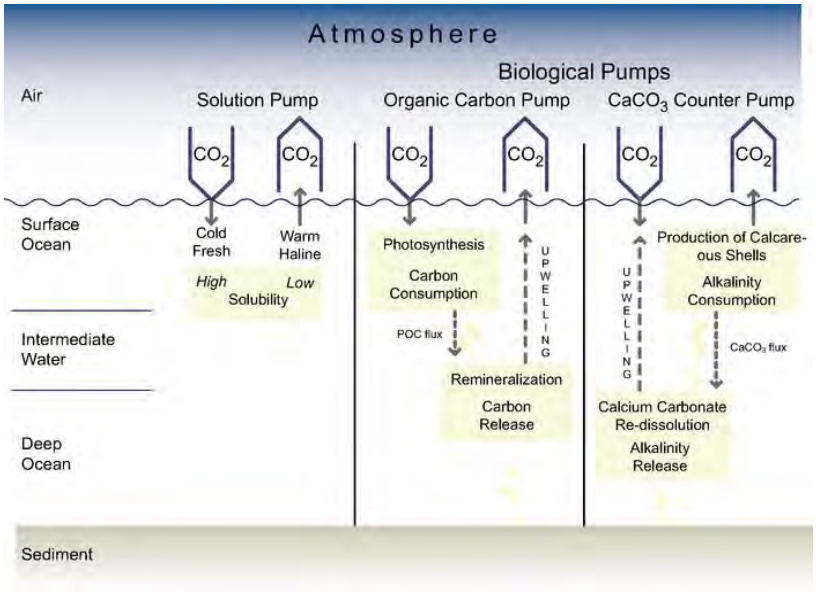

Figure 2.1: Three main ocean carbon pumps govern the regulation of natural atmospheric CO_2 changes by the ocean (Heinze et al, 1991): the solubility pump, the organic carbon pump and the $CaCO_3$ 'counter pump'. The oceanic uptake of anthropogenic CO_2 is dominated by inorganic carbon uptake at the ocean surface and physical transport of anthropogenic carbon from the surface to deeper layers.

Surface oceans are in direct contact with the atmosphere, connecting the deeper water with atmospheric carbon (Sarmiento and Gruber, 2006). The deep ocean carbon reservoir is 25 times larger than the combined carbon reservoirs of the surface ocean and atmosphere (Figure 2.2) (Sigman and Boyle, 2000). The majority of this carbon is stored in the deep oceans as dissolved inorganic carbon. The biological and physical carbon pumps are the mechanisms by which carbon, bound by photosynthesis from the sunlit surface layer, is sequestrated to the deep ocean (Riebesell et al, 2007), where it can be stored for thousands of years.

As atmospheric CO_2 dissolves in seawater, it becomes hydrated to form aqueous CO_2 ($CO_{2(aq)}$), which reacts with water to form carbonic acid (H_2CO_3). It is difficult to distinguish between $CO_{2(aq)}$ and H_2CO_3, thus these two species are combined to express the sum as the concentration of a hypothetical species, $H_2CO_3^*$ (Stumm and Morgan, 1981; Dickson and Goyet, 1994). The hypothetical species dissociates to form bicarbonate (HCO^-_3) and carbonate (CO_3^{2-})

ions, the reaction explained above is represented by the following equation (Figure 2.2) (Skirrow, 1975):

$$CO_2(atm) \leftrightarrow CO_2(aq) + H_2O \leftrightarrow H_2CO_3 \leftrightarrow H^+ + HCO_3^- \leftrightarrow 2H^+ + CO_3^{2-} \quad \text{(Eq 2.1.1)}$$

- The four carbon system parameters are linked through the dissociation constants of carbonic acid:

$$K_O = \frac{[H_2CO_3^*]}{pCO_2(g)} \quad \text{(Eq 2.1.2)}$$

$$K_1 = \frac{[H^+][HCO_3^-]}{[H_2CO_3^*]} \quad \text{(Eq 2.1.3)}$$

$$K_2 = \frac{[H^+][CO_3^{2-}]}{[HCO_3^-]} \quad \text{(Eq 2.1.4)}$$

where K_0, K_1 and K_2 are the equilibrium relationship between the different reactions and are dependent on the sea water temperature and salinity. The squared brackets denote total concentrations and pCO_2 is the partial pressure of carbon dioxide.

The first equilibrium constant (K_0), known as the solubility coefficient of CO_2 in seawater can be calculated using the equation below:

(Eq 2.1.5)

$$\ln(K_o) = A_1 + A_2\left(\frac{100}{T}\right) + A_3 \ln\left(\frac{T}{100}\right) + A_4\left(\frac{T}{100}\right)^2 + S\left[B_1 + B_2\left(\frac{T}{100}\right) + B_3\left(\frac{T}{100}\right)^2\right]$$

where A_1, A_2, A_3, A_4, B_1, B_2 and B_3 are all constants represented in Table 3.4.1 (Weiss, 1974).

The first (K_1) and second (K_2) dissociation constants of carbonic acid in seawater (as represented in Eq.2.1.3 and Eq.2.1.4) are related to pCO_2 and their concentrations expressed in moles per kilogram of seawater remain constant while seawater undergoes changes in temperature and/or pressure, therefore they are conservative properties (Dyrssen and Sillén,

1967). Both equilibrium constants are comprised of bicarbonate and/or carbonate ions, which are the dominant carbon system parameters found in dissolved inorganic carbon and total alkalinity (TA) (Figure 2.2).

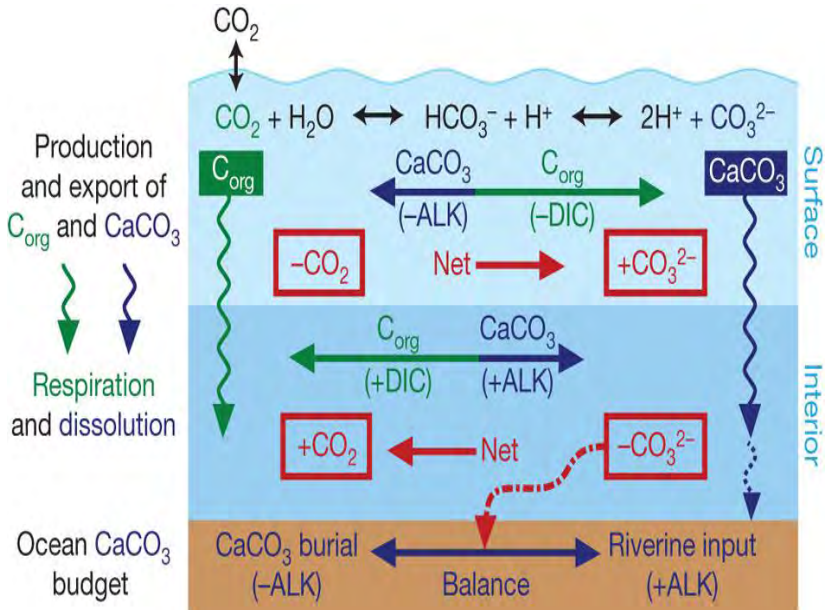

Figure 2.2: The Ocean's inorganic carbon chemistry where bicarbonate is denoted as HCO_3^-, carbonate as CO_3^{2-} and alkalinity as ALK (Sigman et al, 2010).

Dissolved inorganic carbon is a measure of the total amount of inorganic carbon in seawater solution and is controlled by three processes; the biological production, temperature and the air-sea interaction. The most important biological processes altering the concentration of dissolved inorganic carbon in the ocean are the photosynthetic uptake of CO_2 to form organic matter and the reverse processes of respiration and remineralization (Sarmiento and Gruber, 2006). Moreover, only a small fraction of the dissolved inorganic carbon exists as dissolved CO_2; most of the carbon exists as bicarbonate ions and, to a lesser extent, carbonate ions. Thus, dissolved inorganic carbon (DIC) is approximated as the sum of bicarbonate and carbonate ions only (Figure 2.2, Eq 2.1.6).

$$DIC \approx [HCO_3^-] + [CO_3^{2-}] \qquad \text{(Eq 2.1.6)}$$

Total alkalinity is a measure of the excess of bases (proton acceptors) over acids (proton donors) and it is operationally defined by the titration with H^+ of all weak bases present in the seawater solution (Figure 2.2) (Sarmiento and Gruber, 2006).

$$TA = \left[HCO_3^-\right] + 2\left[CO_3^{2-}\right] + \left[B(OH)_4^-\right] + \left[HPO_4^{2-}\right] + \left[OH^-\right] + \left[SiO(OH)_4^-\right].. \\ -\left[H^+\right] - \left[HSO_4^-\right] - \left[HF\right] - \left[H_3PO_4\right] \quad \text{(Eq 2.1.7)}$$

Total alkalinity is made up of three alkalinity variables: water, borate and carbonate alkalinity. Water alkalinity consist of concentrations of hydroxide [OH^-] and hydrogen [H^+] ions; borate alkalinity consist of concentration of borate [$B(OH^-_4)$] ions; and carbonate alkalinity is a sum of the concentration bicarbonate [HCO_3^-] and carbonate 2[CO_3^{2-}] ions (Sarmiento and Gruber, 2006). The distribution of surface alkalinity in the open ocean is mainly controlled by the factors that govern salinity (Broecker and Peng, 1982), because alkalinity is a major component of seawater and the ratio of alkalinity to salinity is nearly constant (Millero et al, 1998). Non-conservative processes, such as precipitation and dissolution of biogenic calcium carbonate ($CaCO_3$) in the water column and in the sediments (Sarmiento and Gruber, 2006), can also contribute to the variability of total alkalinity (Brewer et al, 1975; Brewer and Goldman, 1976). According to Redfield et al (1963) and Park (1969), nutrients and other CO_2 variables such as total inorganic carbon, pH and fugacity of CO_2 (fCO_2), together with biological processes such as photosynthesis and oxidation of organic matter have little direct influence on alkalinity. Variations between the concentration of the minor bases like phosphate, silicate, and sulphate and total alkalinity are usually <1%, and can be ignored, furthermore; the contribution of the dissociation of water to variations in total alkalinity is also negligible, as is the contribution of borate. Therefore, total alkalinity is well approximated by the carbonate alkalinity (Eq. 2.1.8).

$$TA \approx Carbonate\ Alkalinity = [HCO_3^-] + 2[CO_3^{2-}] \quad \text{(Eq 2.1.8)}$$

The continuous uptake of atmospheric CO_2 by the ocean has lowered its pH (=-$\log_{10}[H^+]$) by 0.1 units from pre-industrial levels (Caldeira and Wickett, 2003), thus it is more acidic. Boutin et al (2002) have shown that these chemical changes in seawater will negatively affect ocean organisms such as coccolithophores, foraminifera and pteropods, which, in turn, affects the

stability and probably the production rates of $CaCO_3$ minerals, which are the building blocks for coral reefs and form the exoskeletons of other marine calcifying species. The dissolution of 1 mol of $CaCO_3$ increases dissolved inorganic carbon by 1 mol and total alkalinity by 2 mol (Eq.2.1.6 and Eq.2.1.8), but the remineralization of 1 mol of organic matter increases dissolved inorganic carbon by 1 mol while it decreases total alkalinity by 0.14 mol (16/117), because of the oxidation of organic nitrogen to nitrate (Sarmiento and Gruber, 2006). Ocean acidification may also affect non-calcifying organisms such as viruses and bacteria, although it is yet to be quantified (Iglesias-Rodriguez, 2010).

Extensive research (e.g. see Pérez et al, 2013), has confirmed that the oceans are slowly responding to changes in anthropogenic CO_2. Changes in CO_2 concentrations are noticeable throughout the water column (Sabine et al, 2004) and suggest that full depth measurements are necessary to better understand the role of the oceans in the uptake of CO_2. The Meridional Overturning Circulation (MOC) is the primary mechanism for the storage and transport of carbon, thereby connecting the surface carbon with the huge carbon reservoir of the deep sea.

2.2 Meridional Overturning Circulation (MOC)

The global ocean's ''conveyor belt'' is a simplified conceptual model of the global ocean circulation system consisting of surface and deep water currents, which connect all ocean basins (Figure 2.3). The MOC is responsible in transporting large amounts of water, heat, carbon, salt and nutrients from the tropics to higher latitudes (Speich et al, 2002; Schmittner et al, 2007).

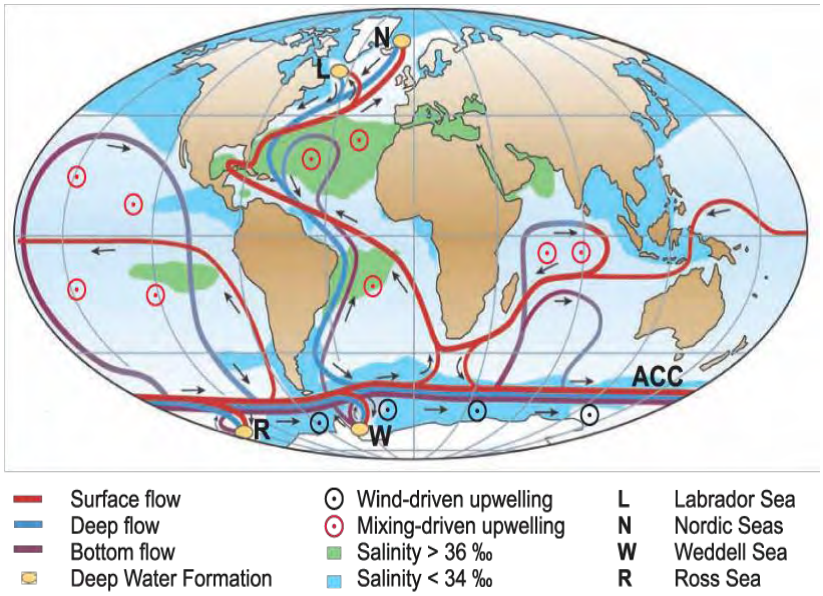

Figure 2.3: Simplified schematic of the Global Overturning Circulation system. The red lines indicate near-surface waters flowing towards four main deep-water formation regions (yellow ovals) in the northern North Atlantic (Labrador-L and Nordic-N Sea), the Ross Sea (R) and the Weddell Sea (W), and recirculates at depth. Deep currents are shown in blue and bottom currents in purple. The green shading indicates salinity above 36 and the blue shading indicates salinity below 34 (Kuhlbrodt et al, 2007).

The physical structure of the MOC belt and its efficiency in regulating climate is substantially influenced by the nature of water mass exchange between ocean basins (Rintoul, 1991; Gordon, 1986). The MOC consists of an upper and a lower branch; the lower branch originates in the vicinity of Iceland where surface flow sinks and returns southwards as North Atlantic Deep Water (NADW) (Broecker, 1991) (Figure 2.3).

The upper branch of the MOC primarily focuses on two routes, cold and warm, that involve totally different water masses (Rintoul, 1991). The cold route (Rintoul, 1991), originates at the Drake Passage, experiencing strong heat gain and evaporation in the Atlantic basin, rendering it more susceptible to variations in the local atmospheric forcing. Meanwhile, the warm route (Gordon, 1986) through the Indonesian Through-flow is subjected to intermittent heat and salt advection by the Agulhas leakage and atmospheric forcing in the Indo-Pacific sector. Over several centuries, changes in the buoyancy of Atlantic, thermocline water masses may have influenced North Atlantic deep-water formation (Weijer et al, 2001), with implications for global climate. According to Biastoch et al (2008), model simulations suggest that a saltier Atlantic ocean, linked to a more efficient leakage of warm and saline Agulhas

waters, leads to a stronger and more stable Atlantic Meridional Overturning Circulation (AMOC).

2.3 Western Boundary Currents

Western boundary currents (WBCs) are intense, narrow flowing currents characterized by strong velocity gradients and a central warm core, with isopycnal lines sloping steeply towards the coast (Bryden et al, 2005; Casal et al, 2009). The three major WBCs of the Southern Hemisphere are the East Australian, Brazil and the Agulhas Currents (Figure 2.4) (Cronin et al, 2010). These WBCs, and the Agulhas Current in particular, interact with the Antarctic Circumpolar Current, especially in the Indian and Atlantic Oceans, whereby heat is transported towards the pole through eddies associated with the WBC poleward extensions (Cronin et al, 2010). All WBCs transport significant amounts of heat, nutrients and carbon to higher latitudes (Atkinson, 2010; Huthnance, 2010) and play a significant role on global climate. According to Xue et al (1995); Kondo (1976) and Rouault and Lutjeharm, (2000) heat loss estimates over the WBCs can range up to 1000 Wm^{-2}.

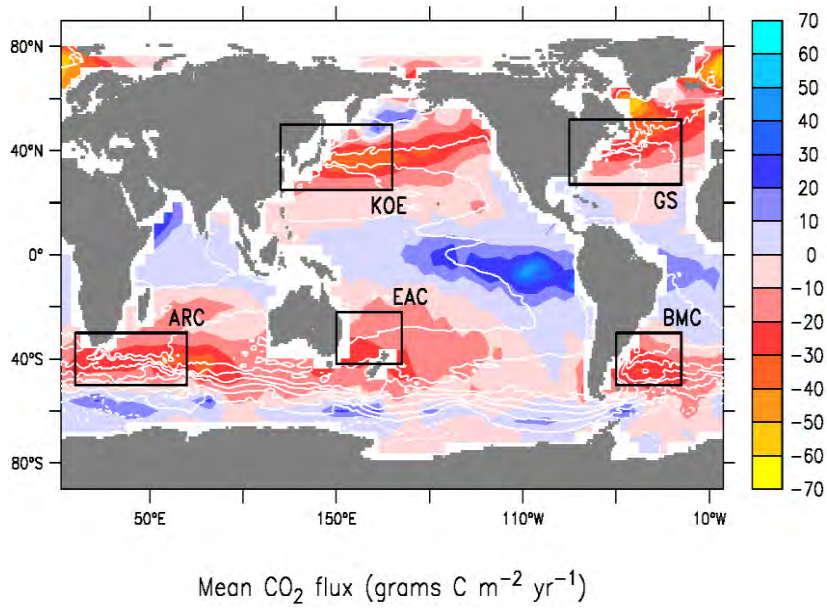

Figure 2.4: Climatological mean annual sea-air CO_2 flux (grams C m^{-2} yr^{-1}) for the western boundary currents for the reference year 2000 (non-El Niño conditions), adapted from Takahashi et al (2007). White contours indicate mean dynamic sea level (Rio and Hernandez, 2004). Agulhas Return Current is abbreviated as ARC; Kuroshio–Oyashio Extension as KOE; East Australian Current as EAC; Gulf Stream as GS and Brazil/Malvinas Current as BMC (Cronin et al, 2010).

2.3.1 The effects of CO_2 on western boundary currents in the Southern Hemisphere.

Globally, WBCs act as sinks of atmospheric CO_2 (Sarmiento and Gruber, 2006). The East Australian, Brazil and the Agulhas Currents have an annual mean CO_2 flux range -20 and -10 gramsC.m^{-2}.y^{-1} increasing by ~ 20 gramsC.m^{-2}.y^{-1} as the currents move away from their origins (Cronin et al, 2010; Figure 2.4). As WBCs extend into the ocean basin, air-sea interactions intensify resulting in more heat and moisture loss from the ocean (through large surface latent and sensible heat fluxes) to the atmosphere. This results in an increase in CO_2 intake (Figure 2.4). The Agulhas Current system in the South Indian Ocean, the East Australian Current system in the South Pacific and the Brazil-Malvinas Confluence in the South Atlantic Ocean have shown that large surface heat loss tends to occur during wintertime when the air is substantially cooler than the sea surface temperature and prevailing winds are predominantly offshore (Rouault et al, 2009). Carbon uptake is associated with wintertime heat loss by WBCs, as sea surface temperature declines; surface water CO_2 concentrations also decrease, increasing the thermodynamic drive for the ocean to absorb CO_2 from the atmosphere (Cronin et al, 2010).

The ocean dynamics south of Africa provides an ideal opportunity to study how changes in the Agulhas Current system influence the uptake of CO_2. Using data collected within the first Crossroads transect occupied in May 2013 across both the Agulhas and the Agulhas Return Currents the nature of CO_2 concentrations and fluxes across this region could be defined. This study improves our understanding of the role WBCs play in the uptake of CO_2.

Key Objectives

The opportunity to collect data across the Agulhas Current system presented itself during the return leg of the 2013 Marion Island Relief Voyage. The cruise provided, for the first time, a high resolution hydrographic transect across both the Agulhas and Agulhas Return Currents. Using underway data collected along this transect the following key objectives aimed at investigating the role of the Agulhas and Return Currents in the uptake of CO_2 will be addressed:

1. To characterize the sub-Tropical region (36 – 38.3 °S), sub-Antarctic region (38.31 – 45 °S) and the Agulhas Current system in terms of CO_2 distribution and uptake.
2. To determine the main mechanism responsible for CO_2 sink within the sub-Tropical region, sub-Antarctic region and the Agulhas Current system.
3. To determine whether the mesoscale feature assumed to have Agulhas Current origins is indeed an Agulhas Plateau eddy and whether the mesoscale feature is a regular feature.

3. Data and Methods

Data used for this study comprises of the 2012 and 2013 return voyages on board the SA Agulhas I and II, the 2013 dataset will be used in the investigation of objectives 1 – 3 and the 2012 dataset will be used to further investigate the third objective. This dataset comprises of a combination of surface underway pCO_2 data, satellite sea surface temperature and Chlorophyll-a data and stationary hydrographic measurements. A limitation of this dataset is that CO_2 measurements were restricted to the surface (5 m) layer and thus do not reflect the entire water column. However, despite this restriction, both cruises provide a unique opportunity to calculate CO_2 fluxes across the Agulhas Current system (Agulhas and Agulhas Return Currents), and their compare to the region south.

In addition, the two datasets will be compared to highlight the variability in fCO_2 between cruises as well as to establish the influence of mesoscale features, considered to be of Agulhas Current origin, lying within the sub-Antarctic domain.

3.1 Physical observations

Two datasets were collected between 36 - 45 °S in April - May 2012 and 2013. The transect runs from Cape Town to the Prince Edward's Islands (Marion and Prince Edward Islands) crossing over the southern-edge of the Agulhas Current through the inner retroflection loop, over the Agulhas Return Current and across the Agulhas Plateau (Figure 3.1). The cruise track transects from a sub-Tropical region, across the sub-Tropical Front into the sub-Antarctic domain. Data was processed using Ocean Data View (ODV; Schlitzer, 2009), MATLAB and Microsoft Excel 2010.

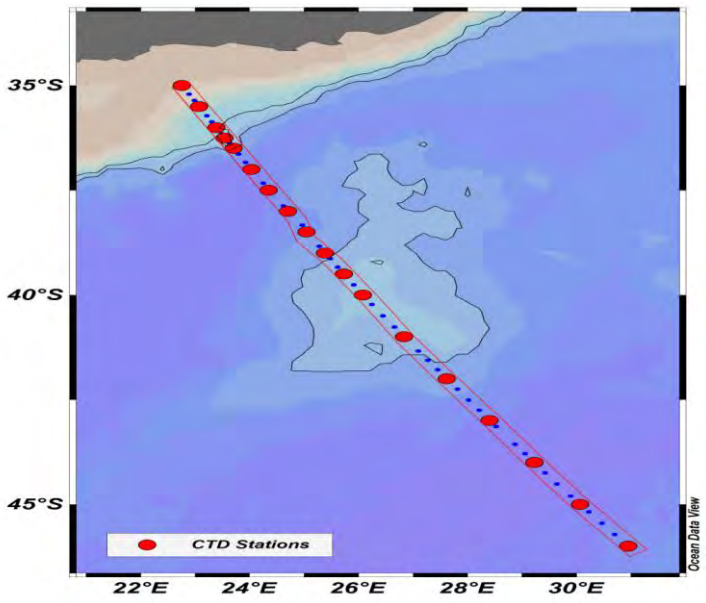

Figure 3.1: Location of hydrographic stations occupied during the 2013 Crossroads transect. The red circles correspond to Conductivity Temperature and Depth (CTD) stations and blue to Expendable BathyThermograph (XBT). The underway pCO_2 system was in operation throughout the entire transect. The black lines represent isobaths at 1000 and 3000m and the area above sea level is shaded in grey.

3.1.1 Crossroads dataset (2013)

A total of 18 full depth Conductivity Temperature and Depth (CTD) stations and 34 Expendable BathyThermograph (XBT) at a 1000 m depth, were deployed along the Crossroads transect (Figure 3.1). The section used in this study extended from the Agulhas Current at 36.25˚S to the southern edge of the Agulhas Plateau at 42.5 ˚S and consisted of 12 CTD stations and 15 XBTs (Figure 3.1). The Agulhas Current was identified using GHRSST satellite sea surface images and the sub-Tropical Front (STF) was identified (using criteria based on Orsi et al, 1995) at 40.49 °S. The CTD stations were full depth and initially at one degree intervals, however due to the energetic nature of the Agulhas Current System it was decided to increase the resolution to every 30' of latitude north of 38 °S. In addition, all standard water and microbial samples were collected at surface, f-max, O_2 min, 200 m and bottom at stations 38 °S, 37 °S and 36 °S. These stations were selected as they best represented stations within the core of the Agulhas Return Current, Agulhas Current and the region between the 2 pathways (referred to as the inner loop) respectively (Figure 3.1; Figure 3.2).

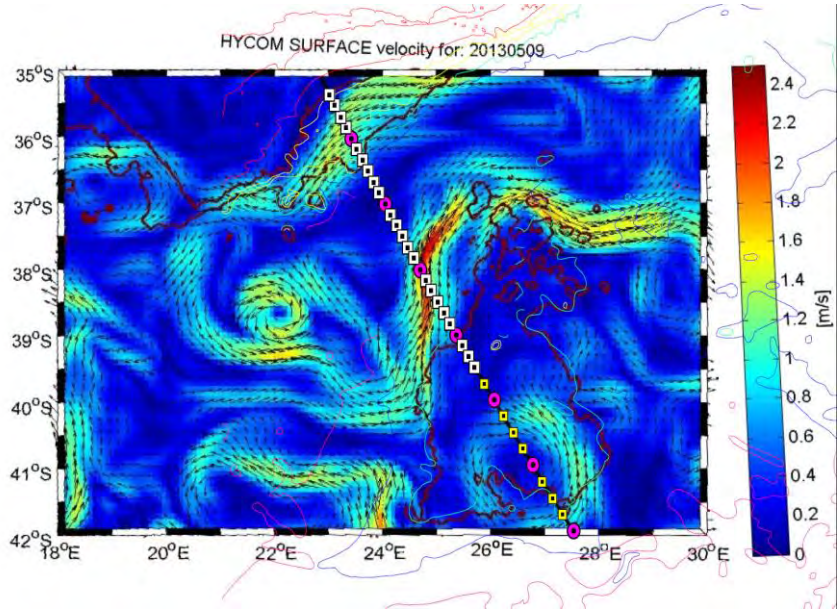

Figure 3.2: Location of the Crossroads line superimposed on the background velocities computed from the Hycom model for April 2013. The pink circles correspond to Conductivity Temperature and Depth (CTD) stations, and the white and yellow squares to Expendable BathyThermograph (XBT). The arrows represents the magnitude and direction of the wind speed, colour on the diagram also represents the magnitude of wind speed (reproduced with permission from Jeff Book).

Acoustic Doppler Current Profiler (ADCP) data was processed using CODAS ADCP processing software (http://currents.soest.hawaii.edu/docs/doc/codas_doc/adcp_processing.html). ADCP measures ocean velocity using the physical principle of Doppler Shift. Three or four acoustic transducers emit acoustic beams at different angles in order to measure ocean velocity in all three directions: north, east and vertical. Each acoustic beam penetrates up to a maximum depth of 750 m. Velocities were obtained from the ship-based ADCP at the time of the survey and ranged from a maximum of 2.5 $m.s^{-1}$ within the core of the Agulhas Return Current to 2 $m.s^{-1}$ within the Agulhas Current and <0.5 $m.s^{-1}$ within the inner loop (Figure 3.3).

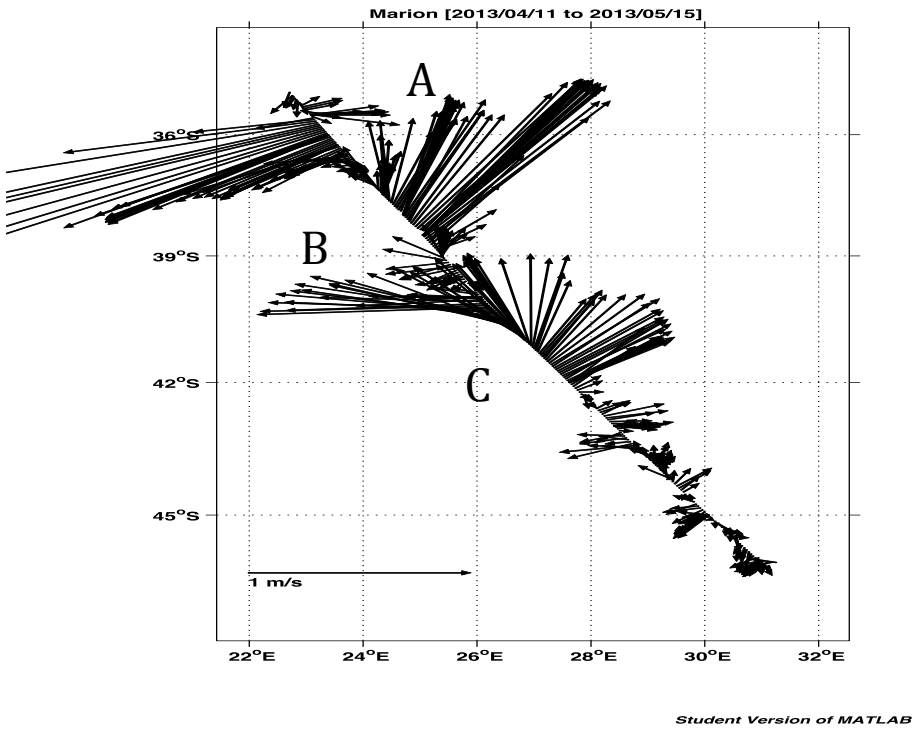

Figure 3.3: ADCP (Acoustic Doppler Current Profile) surface current speed plot along the Crossroads transect. The vectors highlight the position of the westward Agulhas Current (~36.5 °S), its eastward Agulhas Return Current (38.3 °S) and an anticyclonic (41 °S) feature over the Agulhas Plateau.

3.2 Biogeochemical observations

Partial pressure of carbon dioxide (pCO_2) was determined continuously in surface water and in the marine atmosphere with an underway General Oceanics equibrator-based system with a Li-COR LI-7000 infra-red gas analyser, designed after Wanninkhof and Thoning (1993) and described by Pierrot et al (2009). Four reference gases of known CO_2 partial pressures were used: 0, 357.83, 377.5 and 427.83 µatm for 2012 and 0, 314.34, 377.23 and 427.23 µatm for 2013. The instrument was re-calibrated every four hours to these gases (CO_2 partial pressure) followed by atmospheric measurements. Seawater was drawn from a shipboard inlet pump, measuring pCO_2 at 5 m depth and it was directed into an equilibrator where the CO_2 in seawater equilibrates with the gas in the headspace of the chamber (Pierrot et al, 2009). After drying, the gas was then pumped through a non-dispersive infrared analyser (Licor 7000) which instantaneously measures the CO_2 mole fraction (xCO_2) of the gas and atmospheric air was pumped through the analyser and its xCO_2 was determined. Auxiliary instruments logged onto the underway pCO_2 analyser included a Global Positioning System (GPS) and

atmospheric pressure probe situated 5m above the Licor and equilibrator in a deck housing, intake temperature near the keel at 5 m depth, a Turner 10-AU fluorometer, a Fluke digital thermometer to measure the equilibrator temperature, a differential barometer to record the equilibrator pressure relative to atmospheric pressure and an Idronaut multisensor that measures the sea surface temperature and salinity. The pCO_2 data was post processed using the pCO_2 Data Reduction (v109) Matlab Program which calculated the fCO_2 (fugacity of CO_2 in water and atmosphere) data necessary to obtain CO_2 flux value (Pierrot et al, 2009).

3.3 Carbonate system

3.3.1 Alkalinity calculations and verification

Alkalinity data for the Agulhas Current system were obtained by using the equation below (Lee et al, 2006):

$$A_t = a + b(SSS - 35) + c(SSS - 35)^2 + d(SST - 20) + e(SST - 20)^2 \qquad \text{(Eq. 3.3.1a)}$$

where a, b, c, d and e are constants vital for the calculation of alkalinity according to Lee et al (2006). Sea surface temperature (SST) measurements in this system lie between two groups; Group 1: SST > 20 ^{0}C and Group 2: SST < 20 ^{0}C, along with different constants suitable for each temperature group (Table 3.1).

Alkalinity values used in this study were verified by comparing calculated A_t using the Eq. 3.3.1a and observed A_t values obtained from the GoodHope observation line (WOCE_A21/A12 (World Ocean Circulation Experiment)) for the year 1990 over the same latitude (35 - 48.7 °S) which correlated (R^2) to 0.94 (Graph 3.1).

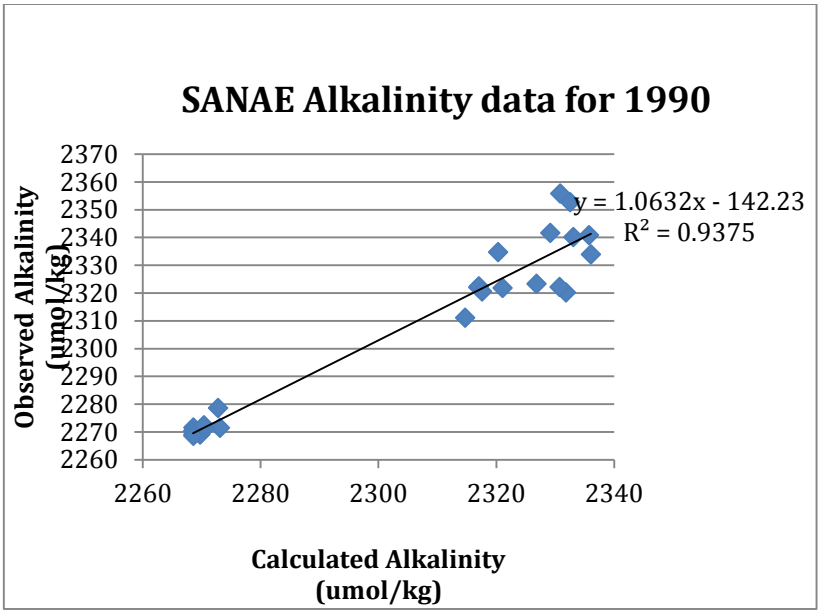

Graph 3.1: Correlation of sampled sea surface alkalinity data against surface calculated alkalinity data obtained using the Lee et al equation (2006). The 1990 dataset was used to correlate observed and calculated total alkalinity, we acknowledge that the dataset is 23 years older than the 2013 dataset but due to lack of observed total alkalinity data in the Southern Hemisphere at similar latitudes to those of this research topic, the 1990 dataset had to be used to obtain the correlation.

Table 3.1: Constants essential for obtaining total alkalinity ($\mu mol.kg^{-1}$) at different sea surface temperature (SST ^0C). The constants a, b, c, d and e are vital for the calculation of alkalinity according to Lee et al (2006).

SST>20 °C	SST<20 °C
a= 2305	a= 2305
b= 58.66	b= 52.48
c= 2.32	c= 2.85
d= -1.41	d= -0.49
e= 0.04	e= 0.086

3.3.2 Dissolved inorganic carbon calculation

Fugacity of carbon dioxide (fCO_2) data obtained from the underway pCO_2 system and the calculated total alkalinity were then used to calculate the remaining carbonate parameters necessary for an Ocean Acidification study using the CO_2SyS programme (Lewis and Wallace,

1998), with constants K_1 and K_2 from Mehrbach et al (1973) refit by (Dickson and Millero, (1987). Thus, datasets of continuous surface water dissolved inorganic carbon were calculated for the Marion Relief Voyages in 2012 and 2013.

3.4 Carbon dioxide flux calculations

The ocean-atmosphere CO_2 flux is a function of the difference in fugacity ($fCO_2^{sw} - fCO_2^{atm}$) measured in µatm, gas transfer velocity (K_W) and solubility coefficient (K_0).

$$FCO_2 = K_0 K_w (fCO_2^{sw} - fCO_2^{atm}) \quad \text{(Eq 3.4.1)}$$

where K_w is a function of wind speed (U) and Schmidt number (S_c) (Wanninkhof, 1992), which is also a function of temperature (T) in ˚C.

Wind speed is a fundamental component in the determination of transfer of gases as it initiates wave formation, which stimulates turbulent mixing and bubbling of seawater.

$$K_w = 0.17U * \left(\frac{S_c}{600}\right)^{-2/3} \quad \text{for U}\leq 3.6\ \text{ms}^{-1} \quad \text{(Eq 3.4.2)}$$

$$K_w = 2.8(U - 3.4) * \left(\frac{S_c}{600}\right)^{-0.5} \quad \text{for } 3.6 < \text{U} \leq 13\ \text{m.s}^{-1} \quad \text{(Eq 3.4.3)}$$

$$K_w = 5.9(U - 8.4) * \left(\frac{S_c}{600}\right)^{-0.5} \quad \text{for U} > 13\ \text{m.s}^{-1} \quad \text{(Eq 3.4.4)}$$

$$S_c = A - BT + CT^2 - DT^3 \quad \text{(Eq 3.4.5)}$$

where A, B, C and D are all constants used to obtain S_c, these constants are represented in Table 3.4.1 (Sarmiento and Gruber, 2006).

U is measured in $m.s^{-1}$, K_w in $cm.hr^{-1}$ and the solubility coefficient (K_0) of CO_2 in seawater given in $molCO_2.l^{-1}.atm^{-1}$. According to Weiss (1974), K_0 is a function of salinity (psu) and temperature (K) demonstrated in the equation below:

$$ln(K_0) = A_1 + A_2\left(\frac{100}{T}\right) + A_3 ln\left(\frac{T}{100}\right) + A_4\left(\frac{T}{100}\right)^2 + S\left[B_1 + B_2\left(\frac{T}{100}\right) + B_3\left(\frac{T}{100}\right)^2\right] \qquad \text{(Eq 3.4.6)}$$

where A_1, A_2, A_3, A_4, B_1, B_2, B_3 are all constants represented in Table 3.3.1 (Sarmiento and Gruber 2006).

Table 3.2: Constants crucial in determining the solubility coefficient and Schmidt number necessary for the calculation of CO_2 flux.

Solubility coefficient (K_0)	Schmidt number (Sc)
A1= -160.7333	A= 2073.1
A2= 215.4152	B= 125.62
A3= 89.8920	C= 3.6276
A4= -1.47759	D= 0.043219
B1= 0.029941	
B2= -0.027455	
B3= 0.0053407	

3.5 Dimensional Analysis

Dimensional analysis is a mathematical system using conversion factors to move from one unit of measurement to another different unit of measurement. For example, we want to calculate CO_2 flux in $mmol.CO_2.m^{-2}.day^{-1}$, so we first need to convert the K_w, K_o and $dfCO_2$ to units that are found in our desired CO_2 flux unit.

$$FCO_2 = K_0 K_w (fCO_2^{sw} - fCO_2^{atm}) \quad \text{(Eq 3.5.1)}$$

$$K_w = cm.hr^{-1} \quad \text{(Eq 3.5.2)}$$
$$= \left(\frac{24}{100}\right) m.day^{-1}$$

$$K_0 = mol.CO_2 l^{-1}.atm^{-1} \quad \text{(Eq 3.5.3)}$$
$$= 10^6 mmol.CO_2.m^{-3}.atm^{-1}$$

$$fCO_2 = \mu atm \quad \text{(Eq 3.5.4)}$$
$$= 10^{-6} atm$$

thus FCO_2 is calculated using the equation below:

$$FCO_2 = 0.24 K_0 K_w (fCO_2^{sw} - fCO_2^{atm}) \quad \text{(Eq 3.5.5)}$$

where 0.24 is the unit conversion constant obtained after converting all units of the variables involved in the FCO_2 equation to $mmol.CO_2.m^{-2}.day^{-1}$. Negative FCO_2 values represent ingassing of dissolved CO_2.

3.6 Satellite data

Wind data used to calculate carbon dioxide flux (FCO_2) was obtained from 6-hourly NOAA Blended Sea Winds between 12 - 15 April 2012 and 10 - 14 May 2013, at a resolution of 0.25^0 (Zhang et al, 2006).

Sea surface chlorophyll-a concentration were obtained from the Giovanni website (http://gdata1.sci.gsfc.nasa.gov/daac-bin/G3/gui.cgi?instance_id=ocean_8day), the ocean colour radiometric data products from SeaWiFS and MODIS were used to produce this image at a 4 km resolution (8-day temporal resolution) during the time of the survey 10 – 15 May 2013. A 7-day sea surface temperature composite image for the same period was obtained from the Colorado Center for Astrodynamics Research (CCAR,

http://eddy.colorado.edu/ccar/data_viewer/contact) website. In this study, the Aqua SST platform was used due to its relatively high resolution of 4 km. Sea surface chlorophyll-a concentration and temperature imagery were used to define the general circulation of the Agulhas Current system at the time of this study.

3.7 Overview of the Agulhas Current region

The main focus of the study is to characterize the Agulhas and the Agulhas Return Currents in terms of CO_2 and to understand their role in the of CO_2 uptake over the region (35 - 41 °S). The Agulhas Current system is typically oligotrophic (low nutrients and low primary productivity) with a minimum and maximum chlorophyll-a concentration of 0.1 and 1 $mg.m^{-3}$ respectively (Figure 3.3a). The region has sea surface temperatures ranging between 16 - 24 °C (Figure 3.3b). In contrast to the currents, the coastline along South Africa shows the highest concentration of chlorophyll-a concentration up to 5 $mg.m^{-3}$ with the lowest observed chlorophyll-a concentration of 0.1 $mg.m^{-3}$ found within the inner retroflection loop (Figure 3.3a).

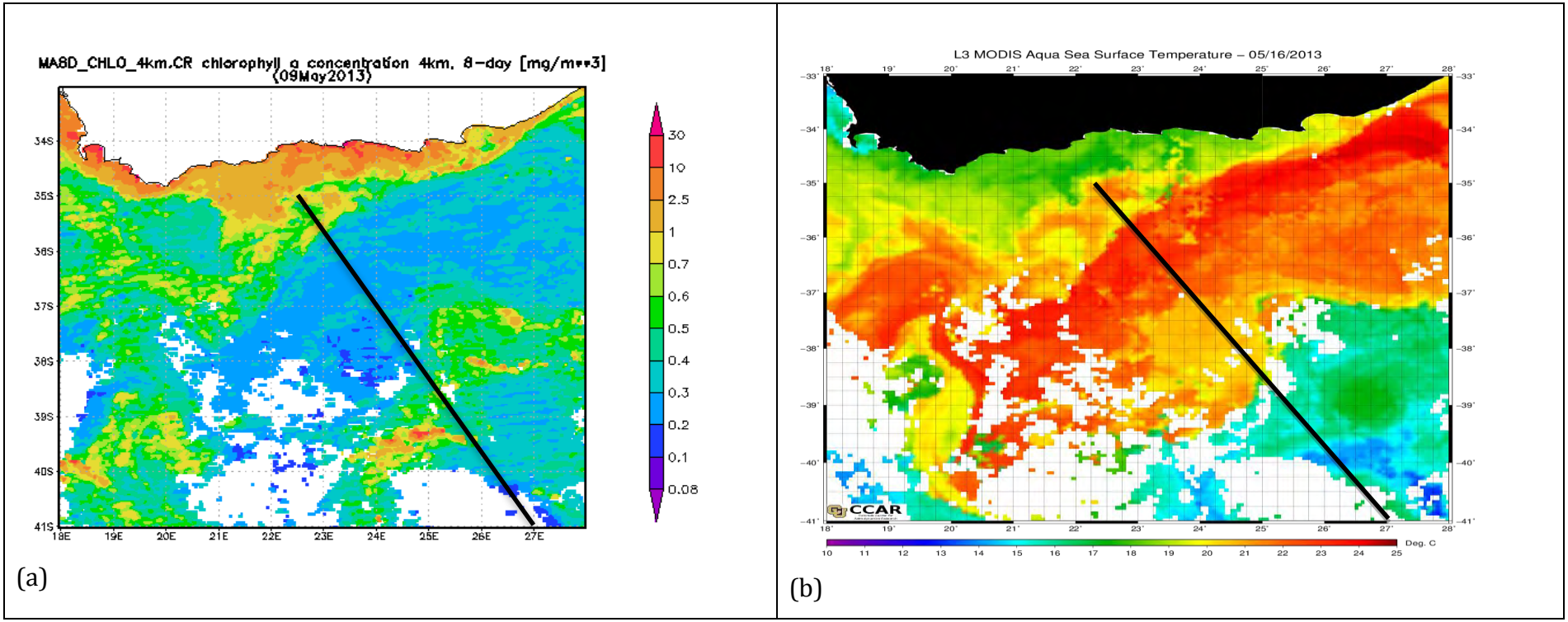

Figure 3.3: Distribution of satellite sea surface chlorophyll-a concentration (a) and temperature (b) between 33 – 41 ˚S. Chlorophyll-a concentration satellite plot was obtained from the Giovanni website, the plot is an 8-day average centred for the 9th May 2013 (http://gdata1.sci.gsfc.nasa.gov/daac-bin/G3/gui.cgi?instance_id=ocean_8day). The sea surface temperature was obtained from the Colorado Center for Astrodynamics Research (CCAR) website, the temperature plot is a 7-day composite (http://eddy.colorado.edu/ccar/data_viewer/contact). The black lines on both plots represents the Crossroads cruise track.

4. Results

The results section will commence with an interpretation of the physical background of the study region, which entails of surface current speeds obtained from the Acoustic Doppler Current Profiler (ADCP) and Temperature/Salinity data collected throughout the water column at a maximum depths of 900 and 1000 m respectively. Examination of the underway pCO_2 data will follow completing the chapter with an interpretation of CO_2 fluxes.

4.1 Regional Oceanography

Temperature and salinity within the sub-Tropical region ranged between 13 – 25 °C (Figure 4.1) and 35.4 - 35.7 respectively, meanwhile further south within the sub-Antarctic region temperatures ranged between 4 – 18 °C (Figures 4.1 and 4.4) and salinity between 33.4 - 35.8 (Figure 4.4). The higher temperature and salinity values of 18 °C and 35.8 in the sub-Antarctic region were the result of an anti-cyclonic eddy assumed to originate from the Agulhas Current region (Figure 4.4). In this study the eddy is referred to as the Agulhas Plateau eddy. The Agulhas Plateau eddy was formed as a result of the interaction of the meandering Agulhas Return Current with the Agulhas Plateau. The eddy circulates over the Agulhas Plateau until it dissipates. Without the Agulhas Plateau eddy maximum temperatures and salinity in the sub-Antarctic zone would have been <15 °C and < 34.7 respectively (Figure 4.4).

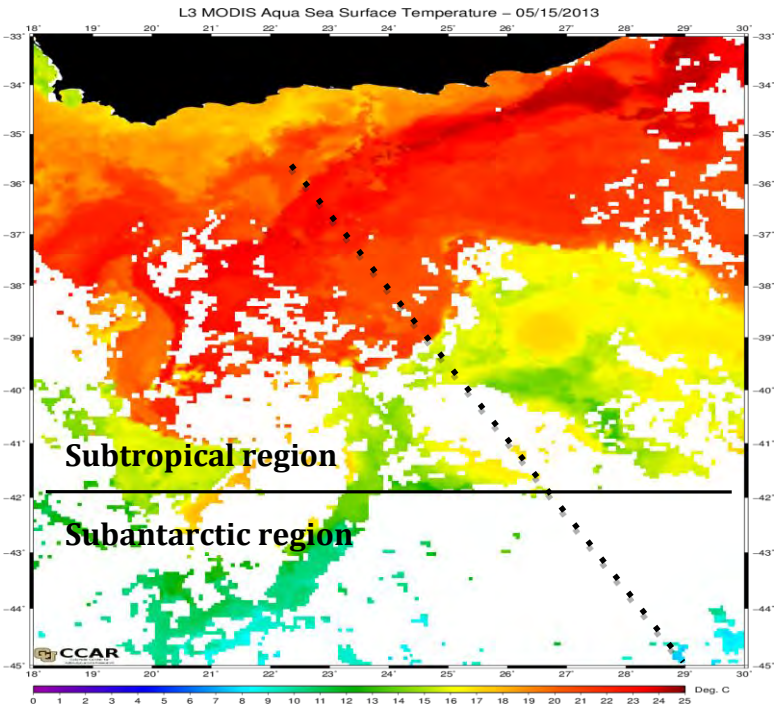

Figure 4.1: Satellite sea surface temperature plot, used to allocate the sub-Tropical and sub-Antarctic regions. The continuous black line indicates the boundary line (i.e sub-Tropical Convergence) between both regions, for this study the continuous line is better suited to demonstrate the sub-Tropical Convergence instead of a meandering line used in literature because the datasets used for this study is station (point) data which does not cover the entire region. The dotted line is the cruise track for May 2013. Satellite sea surface temperature is a 7-day composite obtained from the Colorado Center for Astrodynamics Research (CCAR) website (http://eddy.colorado.edu/ccar/data_viewer/contact).

4.1.1 Advection characteristics

The locations of both Agulhas and Agulhas Return currents at the time of the survey were initially identified from the ship-based ADCP (Acoustic Doppler Current Profiler) velocities (Figure 4.2). The Agulhas Current core was observed from ADCP data to lie at 36.5 °S (Region A) and the Agulhas Return Current at 38.5 °S (Region B) (Figure 4.2). Velocities associated with the Agulhas Current correspond to 2.5 $m.s^{-1}$ while the eastward flowing Agulhas Return Current reached a maximum of ~2 $m.s^{-1}$ (Figure 4.2). These observations are in agreement

with past investigations by Boebel et al (2003), who observed similar velocities of 2.1 $m.s^{-1}$ associated with the Return Current.

In addition, ADCP data showed alternating east and westward flows over the Agulhas Plateau; indicative of an anticyclonic eddy formed it was assumed by the meandering Agulhas Return Current's eastward passage (Figure 4.2). The Agulhas Return Current has been identified to exhibit quasi-stationary meanders comprising of a series crests and troughs, which extend eastwards into the Indian Ocean (Lutjeharms and Ansorge, 2001).

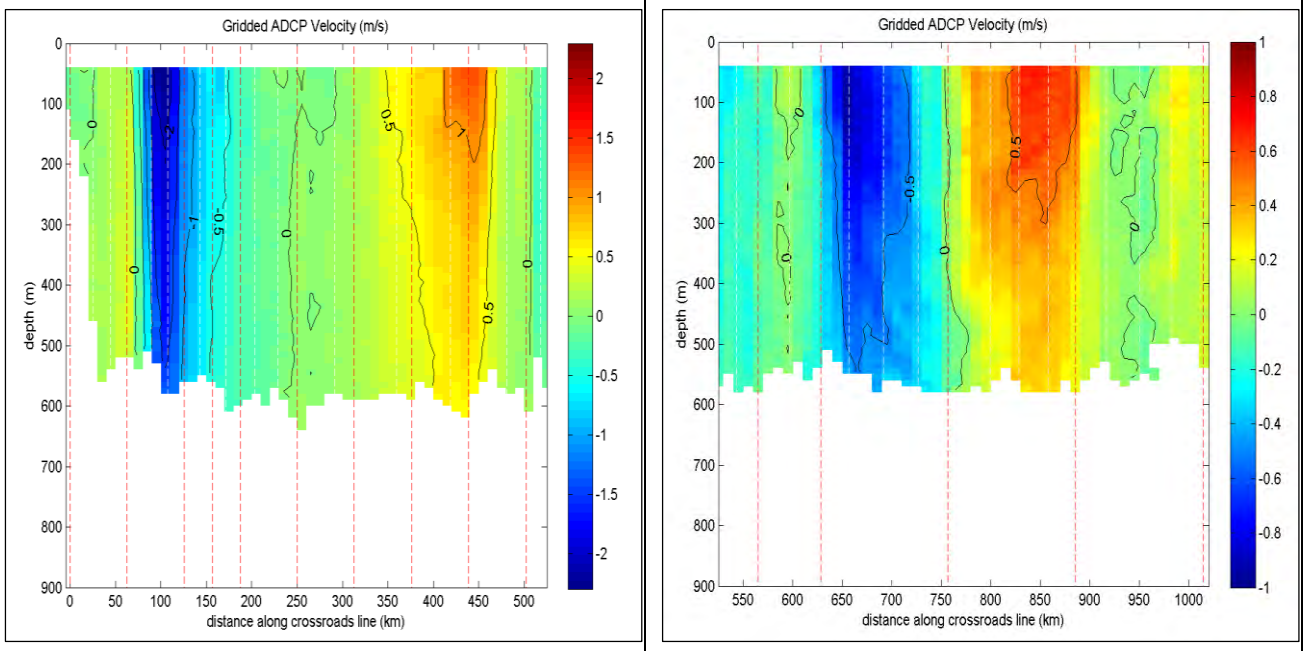

(a) (b)

Figure 4.2: Vertical section showing ADCP data for the top 500 m along the Crossroads line. The first plot highlights the location of the Agulhas Current (blue - negative values) and the Agulhas Return Current (red – positive values) (a) and the plot highlights the position and anticyclonic rotation associated with the eddy overlying the Agulhas Plateau (b).

4.1.2 Temperature-Salinity

Hydrographic stations occupied along the Crossroads transect confirm that surface temperature and salinity observed over the Agulhas Current ranged between 17 – 25 °C and 35.25 – 35.6. Stations occupied within the core of the Agulhas Return Current, displayed similar surface salinities but surface temperatures were cooler ranging between 15 – 22.5 °C (Figure 4.3). Over the Agulhas Plateau and south of the Agulhas Return Current a mesoscale feature consistent with Agulhas water masses (Lutjeharms and Ansorge, 2001) had a maximum temperature of 16 °C and salinities of 35.5 and thus typical of sub-Tropical waters. The section separating the Agulhas Current and its return flow is known as the Inner Retroflection Loop (IRL). At the time of the Crossroads transect this section was observed at a core position of 37 °S and showed a strong temperature gradient of 4 °C (Figure 4.3), indicative of the southern boundary of the Agulhas Current (Lutjeharms and Ansorge, 2001).

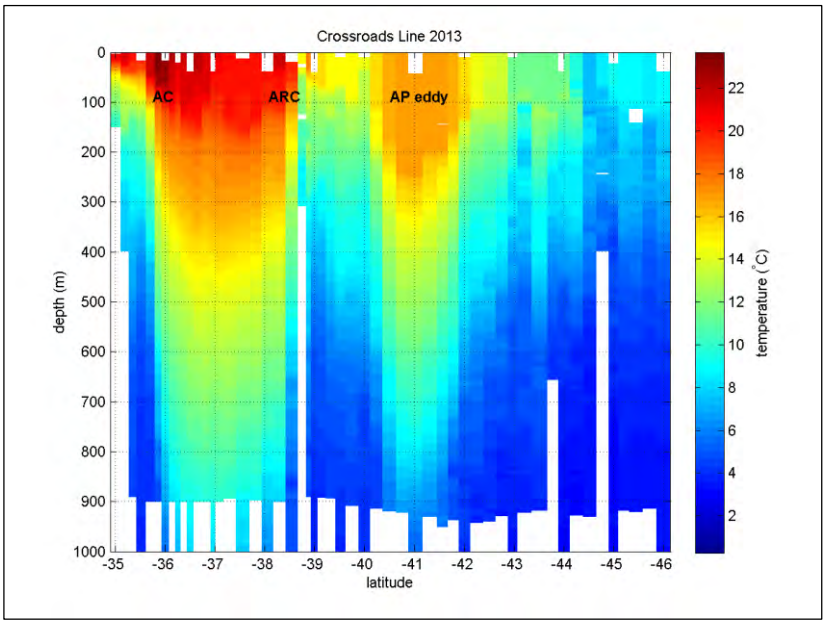

Figure 4.3: Temperature section plot along the Crossroads transect through the water column (0 - 1000 m), where AC is the Agulhas Current, ARC is the Agulhas Return Current and AP is the Agulhas Plateau eddy over the Agulhas Plateau. The region between AC and ARC was denoted as the inner retroflection loop lies between 37 – 37.8 °S.

According to Weiss (1974), the geographical variation of CO_2 penetration in the ocean is mainly due to the increase of solubility with gradually decreasing temperatures as well as the drawdown of surface water masses into the deep ocean. Their findings imply that CO_2 uptake in the Agulhas Return Current is expected to exceed that of the Agulhas Current due to temperature differences. Characterization of the Agulhas Current system in terms of CO_2 required us to determine how CO_2 parameters vary in the Agulhas Current system. In order to characterize the Agulhas Current and its return flow, the sub-Tropical and sub-Antarctic zones will first be characterized with reference to CO_2.

4.2 Surface - underway biogeochemical data

4.2.1 Sub-Tropical Zone

The sub-Tropical zone was located between 36 – 38.4 ˚S (Figure 4.4) and consists of the Agulhas Current system (Agulhas and the Agulhas Return Currents). The zone is warm and saline, temperature ranged between 20 – 22.5 ˚C with a mean value of 21.00 ˚C and salinity ranged between 35.4 – 35.53 with a mean value of 35.5 (Table 4.1, Figure 4.4). Furthermore, the zone is oligotrophic thus mean chlorophyll-a concentration of 0.4 $mg.m^{-3}$ was expected (Figure 4.4).

Table 4.1: Surface mean values of temperature (°C), salinity (psu), dissolved inorganic carbon (µmol.kg^{-1}), total alkalinity (µmol.kg^{-1}) *and* $dfCO_2$ *gradient (*µatm*) in the sub-Tropical and sub-Antarctic zones during the April/May 2013 Prince Edward's Islands cruise.*

Zone	Temperature (˚C)	Salinity (psu)	Dissolved inorganic carbon (µmol.kg^{-1})	Total alkalinity (µmol.kg^{-1})	$dfCO_2$ (µatm)
Sub-Tropical	21	35.5	2034.5	2336	-42.5
Sub-Antarctic	13.73	34.46	2045	2288	-49

The underway data also reflected the biogeochemical (CO_2 and chlorophyll-a) characteristics of the sub-Tropical zone. Dissolved inorganic carbon had a concentration range between 2019 - 2050 µmol.kg^{-1} (Figure 4.4) with a mean value of 2034.5 µmol.kg^{-1} (Table 4.1) and chlorophyll-a concentration ranged between 0.2 - 0.5 $mg.m^{-3}$ (Figure 4.4). Total alkalinity, derived from the Lee et al (2006) method, ranged between 2330 – 2342 µmol.kg^{-1} (Figure 4.4)

with a mean value of 2336 µmol.kg^{-1} (Table 4.1). The dfCO_2 gradient ranged between -66 and -19 µatm with mean value of -42.5 µatm (Table 4.1).

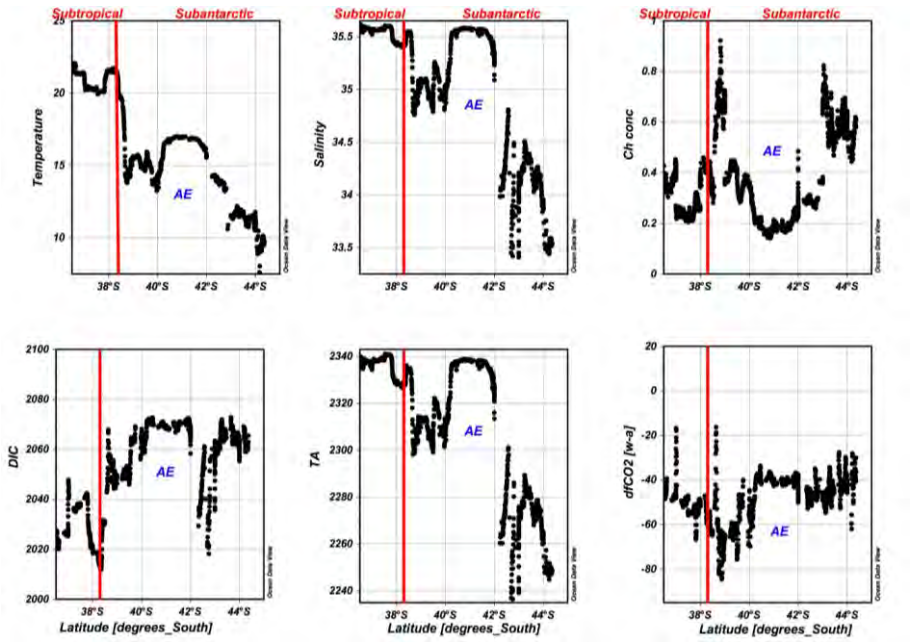

Figure 4.4: Surface underway property plots of the line from Cape Town to Marion Island for the year 2013, depicting temperature in ^{0}C (a), salinity in psu (b), chlorophyll-a concentration (Ch conc) in mg.m^{-3} (c), DIC (dissolved inorganic carbon) (d), TA (total alkalinity) (e) and dfCO_2 [w-a](exchange of CO_2 between the ocean and the atmosphere, in µatm) (f). Total alkalinity and dissolved inorganic carbon both measured in µmol.kg^{-1}. Positive dfCO_2 [w-a] values (>0 µatm) indicate CO_2 outgassing by the ocean and negative values (<0 µatm) CO_2 ingassing. AE and the red line represents the Agulhas Plateau Eddy and the boundary line between sub-Tropical and sub-Antarctic waters, respectively.

4.2.2 Sub-Antarctic zone (SAZ)

The sub-Antarctic zone was observed between 38.4 – 45 ˚S (Figure 4.4). The zone was divided into two smaller zones; the Northern and Southern zones due to presence of the Agulhas Plateau eddy formed by the interaction of the Agulhas Return Current with the Agulhas

Plateau, the eddy was situated between 40 – 42 °S. In addition, the Northern zone was defined as the area before the Agulhas Plateau eddy between 38.6 – 39.8 °S and the Southern zone as the area after the Agulhas Plateau eddy between 42.2 – 45 °S (Figure 4.4).
Both Northern and Southern zones will be addressed in this chapter and the Agulhas Plateau eddy will only be examined in detail in Chapter 5.

Temperature and salinity in the sub-Antarctic zone ranged between 7 – 17.5 ˚C and 33.4 – 35.52, with mean values of 13.73 ˚C and 34.46 respectively (Table 4.1, Figure 4.4). Furthermore, the mean surface temperature and salinity values in the Agulhas Plateau eddy was 16.54 ˚C and 35.3 respectively, which caused temperature and salinity in the sub-Antarctic zone to increase to maximum values of 17.5 ˚C and 35.52 respectively (Figure 4.4).
Dissolved inorganic carbon ranged between 2020 – 2070 $\mu mol.kg^{-1}$ with a mean value of 2045 $\mu mol.kg^{-1}$ and total alkalinity calculated from the Lee et al (2006) ranged between 2238 – 2338 $\mu mol.kg^{-1}$ with a mean value of 2288 $\mu mol.kg^{-1}$ (Figure 4.4, Table 4.1). Additionally, $dfCO_2$ gradient ranged between -79 and -19 µatm (Figure 4.4) with a mean value of -49 µatm (Table 4.1).

A sharp decrease in temperature and salinity across the boundary line at 38.3 °S was expected, because south of the 38.3° latitude warm-salty sub-Tropical surface waters interacts and mix with cool-less salty sub-Antarctic surface waters, which resulted in a 6 °C (from 20 to 14 °C) temperature decrease and 0.75 (from 35.5 to 34.75) salinity decrease between 38.3 – 38.4 °S (Figure 4.4). Additionally, these changes in temperature and salinity resulted in 12.5 - 16 °C temperature range and 34.75 – 35.25 salinity range in the Northern zone. Temperature and salinity in the Northern zone decreased by ~3.5 °C and 0.5 respectively. Additionally, total alkalinity decreased by 21 $\mu mol.kg^{-1}$ and dissolved inorganic carbon increased by 25 $\mu mol.kg^{-1}$ in the same region (Figure 4.4). The $dfCO_2$ gradient and chlorophyll-a concentration in ranged between -83 and -19 µatm, and 0.3 – 0.9 $mg.m^{-3}$ respectively (Figure 4.4). Furthermore, the

mean chlorophyll-a concentration and $dfCO_2$ gradient values were 0.6 $mg.m^{-3}$ and -51 µatm (Figure 4.4).

Temperature and salinity in the Southern zone ranged between 7 – 15 °C and 33.4 - 34.8 respectively (Figure 4.4). Additionally, dissolved inorganic carbon and total alkalinity ranged between 2020 – 2050 $\mu mol.kg^{-1}$ and 2239 – 2300 $\mu mol.kg^{-1}$ (Figure 4.4). Chlorophyll-a concentration and $dfCO_2$ ranged between 0.25 – 0.82 $mg.m^{-3}$, and -55 and -28 µatm (Figure 4.4).

Chapter 4.1 highlighted the oceanographic context (such as, temperature-salinity and advective characteristics) and the differences between CO_2 parameters in the sub-Tropical and sub-Antarctic zones, but the role the Agulhas Current and its return flow have in characterizing CO_2 concentrations within this region remains undescribed.

4.2.3 Agulhas Current system: Agulhas Current, Inner Retroflection Loop and Agulhas Return Current

The Agulhas Current system consist of three regimes of spatial variability; the Agulhas Current, Inner Retroflection Loop (IRL) and the Agulhas Return Current. The Agulhas Current was located between 36.5 – 37 ˚S with the latitudinal boundary line at 37 ˚S, IRL between 37 – 37.9 ˚S with the latitudinal boundary line at 37.9 ˚S and the Agulhas Return Current between 37.9 – 38.5 ˚S (Figure 4.5).

Agulhas Current

Dissolved inorganic carbon in the Agulhas Current region ranged between 2020 – 2030 µmol.kg^{-1} and temperature between 21.5 – 22.1 ˚C (Figure 4.5). Moreover, salinity and total alkalinity ranged between 35.55 – 35.62 and 2335 – 2340 µmol.kg^{-1}. The mean temperature and dissolved inorganic carbon was 21.52 ˚C and 2025 µmol.kg^{-1} (Table 4.2). The mean salinity and total alkalinity values were 35.6 and 2337.5 µmol.kg^{-1}.

Table 4.2: Surface mean values of temperature (°C), salinity (psu), dissolved inorganic carbon (µmol.kg^{-1}), total alkalinity (µmol.kg^{-1}) *and dfCO$_2$ gradient (*µatm*) for the Agulhas Current, Inner Retroflection Loop and the Agulhas Return Current during the April/May 2013 Prince Edward's Islands cruise.*

Region	Temperature (˚C)	Salinity (psu)	Dissolved inorganic carbon (µmol.kg^{-1})	Total alkalinity (µmol.kg^{-1})	dfCO$_2$ (µatm)
Agulhas Current	21.52	35.6	2025	2337.5	-45
Inner Retroflection Loop	20.68	35.53	2033.5	2335.5	-58
Agulhas Return Current	20.75	35.5	2022	2331.1	-56.5

Temperature at ~36.6 ˚S increased by 0.5 ˚C (from 21.5 to 22 ˚C) causing dissolved inorganic carbon to decrease by 8 μmol.kg^{-1} (from 2028 to 2020 μmol.kg^{-1}) (Figure 4.5). Salinity also decreased by 0.08 (from 35.62 to 35.54) resulting in a 5 μmol.kg^{-1} (from 2340 to 2335 μmol.kg^{-1}) decrease of total alkalinity (Figure 4.5). Chlorophyll-a concentration ranged between 0.3 - 0.45 mg.m^{-3} and dfCO_2 gradient between -50 and -40 μmol.kg^{-1} (Figure 4.5) with a mean -58 μatm (Table 4.2).

Inner Retroflection Loop (IRL)

Temperature and dissolved inorganic carbon ranged between 20 – 20.5 ˚C and 2025 – 2042 μmol.kg^{-1} (Figure 4.5). Furthermore, the mean values for temperature and dissolved inorganic carbon were 20.68 ˚C and 2033.5 μmol.kg^{-1} (Table 4.2). Little variability in temperature was observed, resulting in a small temperature range difference of 0.5 ˚C. Chlorophyll-a concentration ranged between 0.2 – 0.3 mg.m^{-3} and dfCO_2 gradient between -68 and -48 μatm (Figure 4.5) with a mean value of -58 μatm (Table 4.2). Total alkalinity and salinity ranged between 2330 – 2341 μmol.kg^{-1} and 35.45 – 35.6 (Figure 4.5) with mean salinity value of 35.53 and mean total alkalinity value of 2335.5 μmol.kg^{-1} (Table 4.2).

Agulhas Return Current

The lowest dissolved inorganic carbon ranged between 2012 – 2031 μmol.kg^{-1} in the Agulhas Current system was observed in this region between a temperature range of 19.8 – 21.5 ˚C (Figure 4.5). Furthermore, the mean temperature and dissolved inorganic carbon values were 20.75 ˚C and 2022 μmol.kg^{-1} (Table 4.2). Salinity and total alkalinity ranged between 35.4 –

35.55 and 2327.5 – 2335.1 µmol.kg^{-1} (Figure 4.5). Moreover, the mean salinity and total alkalinity values were 35.5 and 2331.1 µmol.kg^{-1}. DfCO_2 gradient ranged between -65 and -48 µatm and had a mean value of -56.5 µatm (Figure 4.5, Table 4.2). Chlorophyll-a concentration in this region was the same as that found in the Agulhas Current region and had a concentration range between 0.3 – 0.45 mg.m^{-3} (Figure 4.5).

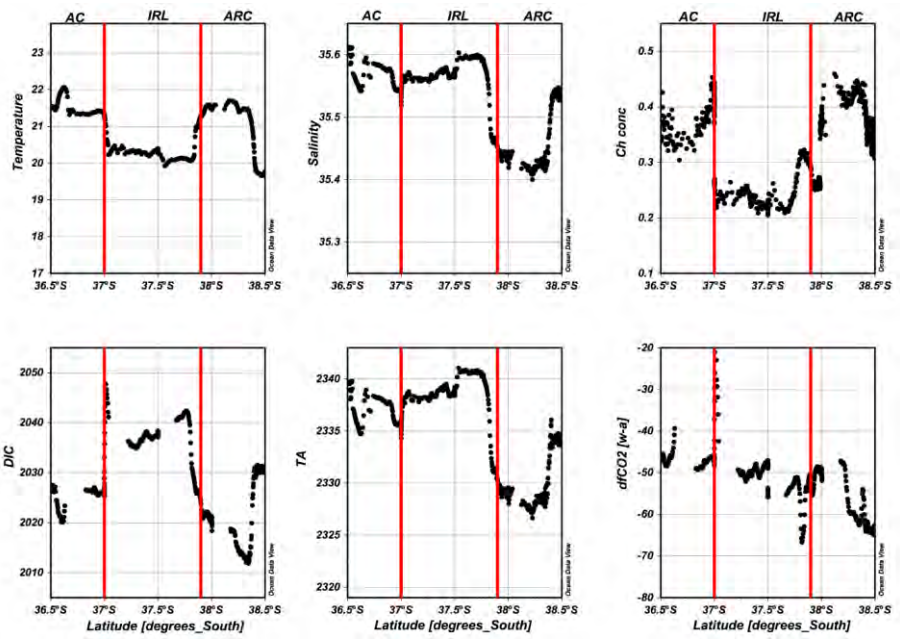

Figure 4.5: Surface underway property plots for the Agulhas Current (AC), the Inner Retroflection Loop (IRL) and the Agulhas Return Current (ARC) for the year 2013; demonstrating temperature in ^{0}C (a), salinity in psu (b), chlorophyll-a fluorescence (Ch conc) in mg.m^{-3} (c), DIC (dissolved inorganic carbon) (d), TA (total alkalinity) (e) and dfCO_2 [w-a](exchange of CO_2 between the ocean and the atmosphere, in µatm) ((f). Total alkalinity and dissolved inorganic carbon both measured in umol.kg^{-1}. Positive dfCO_2 [w-a] values (>0 µatm) indicate CO_2 outgassing by the ocean and negative values (<0 µatm) CO_2 ingassing. The two red lines represent the boundary lines between the AC, IRL and the ARC.

4.3 CO_2 fluxes

In order to establish the mechanism responsible for the CO_2 sink, the variables responsible for obtaining CO_2 flux need to be investigated. Temperature, $dfCO_2$ gradient and wind speed are the three variables vital for obtaining the magnitudes of CO_2 sink in the sub-Tropical zone, sub-Antarctic zone and the Agulhas Current system (Agulhas and Agulhas Return Currents). Temperature is a proxy for the solubility coefficient and wind speed is a proxy for the gas transfer velocity of CO_2.

The sub-Tropical zone had a mean CO_2 flux of -4.92 $mmolC.m^{-2}.day^{-1}$ as a result of average $dfCO_2$ value of -49.28 µatm, wind speed of 8.25 $m.s^{-1}$ and a mean temperature value of 21 °C (Table 4.3). Similarly, the sub-Antarctic zone also had a similar wind speed of 8.87 $m.s^{-1}$, $dfCO_2$ gradient of -51 µatm and a mean temperature of 13.73 °C that resulted in a mean CO_2 flux of -5.89 $mmolC.m^{-2}.day^{-1}$ (Table 4.3).

Table 4.3: Surface mean values and standard error of $dfCO_2$ (µatm), temperature (°C), wind speed ($m.s^{-1}$) and CO_2 flux ($mmolC.m^{-2}.day^{-1}$) for the sub-Tropical; sub-Antarctic zone, Agulhas current (AC), Inner Retroflection loop (IRL), Agulhas Return Current (ARC) and the Agulhas Plateau eddy (AE) during April/May Prince Edward's Islands cruise track for 2013.

	Mean $dfCO_2$ (µatm)	**Mean wind speed ($m.s^{-1}$)**	**Mean temperature (°C)**	**Mean CO_2 flux ($mmolC.m^{-2}.day^{-1}$)**
2013:				
Sub-Tropical	-49.28 ± 4.81	8.25 ± 0.90	21.00 ± 0.57	-4.92 ± 1.06
Sub-Antarctic	-51.00 ± 12.44	8.87 ± 1.24	13.73 ± 3.21	-5.89 ± 1.72
AC	-47.06 ± 1.71	7.26 ± 0.34	21.52 ± 0.23	-3.73 ± 0.39
IRL	-49.24 ± 5.63	8.68 ± 0.61	20.68 ± 0.50	-5.34 ± 0.79
ARC	-56.59 ± 6.66	8.67 ± 1.24	20.75 ± 0.87	-6.30 ± 2.07
AE	-41.68 ± 5.11	12.23 ± 1.70	16.54 ± 0.72	-8.12 ± 1.89

The Agulhas Current had a mean CO_2 flux of -3.73 $mmolC.m^{-2}.day^{-1}$ as a result of 7.26 $m.s^{-1}$ wind speed, mean temperature value of 21.52 °C and a mean $dfCO_2$ gradient of -47.06 µatm (Table 4.3). Moreover, the Agulhas Return Current had a mean temperature value of 20.75 °C; $dfCO_2$ mean value of -56.59 µatm and mean wind speed value of 8.67 $m.s^{-1}$ resulting in CO_2 flux of -6.30 $mmolC.m^{-2}.day^{-1}$. The IRL had similar mean wind speed and temperature values as the Agulhas Return Current region (Table 4.3). Furthermore, mean $dfCO_2$ and CO_2 flux were -49.24 µatm and -5.34 $mmolC.m^{-2}.day^{-1}$.

5. Discussion

According to Sabine et al (2004), recent uptake of heat by the ocean has led to a significant increase in sea surface temperatures in both the Tropics and mid-latitudes. Warming of the surface layers has been observed in the Tropical Indian Ocean and over the deep-water formation region in the high-latitudes (Sabine et al, 2004; Gille, 2014). Moreover, excess evaporation in both regions increased the salinity and density of the waters, resulting in an increase in the drawdown of anthropogenic CO_2 (Sabine et al, 2004; Gille, 2014). Takahashi et al (2009) added that the southern Tropical and sub-Tropical Indian Ocean is a moderate sink of atmospheric CO_2, with ~0.4 Peta grams of carbon (PgC) per year. The CO_2 sink in this area was essentially associated with the solubility pump, because the annual mean biological production was minimal typical of sub-Tropical gyres (Figure 3.4) (McClain et al, 2004).
The first objective of this study was to investigate the differences of CO_2 characteristics between sub-Tropical zone, sub-Antarctic zone and within the Agulhas Current system (Agulhas and Agulhas Return Currents). A second objective is aimed at examining the main mechanism (solubility or biological pump) responsible for oceanic uptake of CO_2 in these regions and how they differed from one another?

5.1 What are the differences in the CO_2 sink in the sub-Tropical and sub-Antarctic zones?

To address this question, differences in CO_2 parameters such as $dfCO_2$, total alkalinity and dissolved inorganic carbon are discussed in detail.
The sub-Tropical zone is made up of the Agulhas Current system (Agulhas and the Agulhas Return Currents), therefore the region is warm-saline and oligotrophic. Additionally, the zone had maximum temperature and salinity values of 22.5 ˚C and 35.53 (Figure 4.4). The

maximum chlorophyll-a concentration in the sub-Tropical zone was 0.5 $mg.m^{-3}$, which was in support with the findings obtained by Thomalla et al (2011) that stated that chlorophyll-a concentrations north of the Agulhas Front did not exceed 0.2 $mg.m^{-3}$, meanwhile south of the Agulhas Front; a maximum concentrations of 0.4 $mg.m^{-3}$ were associated with the sub-Tropical Front. The sub-Tropical zone is oligotrophic due to its high-nutrient low-chlorophyll nature, resulting in a low mean chlorophyll-a concentration value of 0.3 $mg.m^{-3}$ (Figure 4.4). Furthermore, the high temperatures known to enhance phytoplankton growth and photosynthesis, were reduced by the lack of nutrients (such as phosphate etc.), iron and silicic acid, thus resulting in low chlorophyll concentration (Thomalla et al, 2011).

Dissolved inorganic carbon in the sub-Tropical zone increased from 2020 to 2050 $\mu mol.kg^{-1}$ across the Agulhas Current region (36.5 - 37 °S) causing a decrease in $dfCO_2$ gradient from -50 to -19 µatm (Figure 4.4). The increase in dissolved inorganic carbon was a result of temperature decreasing by 2.5 ˚C (from 22.5 to 20 ˚C) as the current progressed south into cooler Atlantic surface waters within the Agulhas retroflection region (Figure 4.4).

Dissolved inorganic carbon in the northern (at 36.5 °S) and southern edge (~38.4 °S) of the sub-Tropical zone was relatively low at values of 2020 and 2010 $\mu mol.kg^{-1}$ respectively (Figure 4.4). Additionally, $dfCO_2$ gradient for the northern edge was -40 µatm whilst the southern edge was -70 µatm. Primary production was responsible for the relatively low dissolved inorganic carbon values that results in low $dfCO_2$ gradient, during photosynthetic processes both dissolved inorganic carbon and nutrients are consumed in order to produce chlorophyll concentration. The relatively high $dfCO_2$ gradient in the southern edge was unexpected, but was a result of the 10 $\mu mol.kg^{-1}$ (2340 – 2330 $\mu mol.kg^{-1}$) decrease in total alkalinity. Decreasing total alkalinity increases fCO_2 that in turn decreased dissolved inorganic carbon confirming that primary production did occur resulting in maximum chlorophyll-a concentration value of 0.4 $mg.m^{-3}$ in the southern edge.

On average, temperatures across the sub-Tropical zone deviated from its mean by 0.6 ˚C (Table 4.3), suggesting that temperature variability might be one of the major variables responsible for air-sea exchange of carbon. The increase of $dfCO_2$ gradient from -40 to -66 µatm agreed with Sarmiento and Gruber (2006) statement that stated that decreasing temperature will result in an increase in dissolved inorganic carbon in the absence of biological processes, thus increasing the air-sea exchange of CO_2. In this case $dfCO_2$ gradient increased by a magnitude of 26 µatm that resulted in a mean carbon sink of -4.92 $mmol.C.m^{-2}day^{-1}$ (Figure 4.4, Table 4.3).

Crossing the sub-Tropical Convergence (STC, boundary line) at 38.3 °S into the sub-Antarctic zone, a sharp drop in temperature and salinity between 38.4 – 38.5 °S occurred resulting in dilute and cooled surface waters due to mixing caused by the meandering STC. Additionally, temperature decreased from 20 to 13.8 °C and salinity from 35.5 to 34.75, these changes were expected when progressing from warmer sub-Tropical waters into cooler sub-Antarctic surface waters (Figure 4.4). Thus, a decrease in temperature resulted in an increase in dissolved inorganic carbon from 2040 to 2070$\mu mol.kg^{-1}$, which was expected because the relationship between temperature and dissolved inorganic carbon in the absence of biological processes is inversely proportional. Additionally, the decrease in salinity resulted in a decrease in total alkalinity from 2327 to 2300 $\mu mol.kg^{-1}$ as a result of the direct relationship between salinity and alkalinity (Figure 4.4) (Lee et al, 2006).

Temperature; salinity, dissolved inorganic carbon and total alkalinity plot in Figure 4.4 showed spatial variability in the Northern zone (38.6 – 39.8 °S), due to mixing effects caused by the STC at 38.4 °S and the presence of the Agulhas Plateau eddy southwards. Temperature and salinity increased to a maximum value of 16 °C and 35.25 (Figure 4.4). The variability in dissolved inorganic carbon resulted in $dfCO_2$ gradient decreasing from -82 to -40 µatm.

Chlorophyll-a concentration reached a maximum concentration of 0.9 $mg.m^{-3}$ (Figure 4.4), suggesting that photosynthesis was important in this zone. Furthermore, the maximum concentration corresponded with a decreased dissolved inorganic carbon value of 2045 $\mu mol.kg^{-1}$ at 39 °S due to photosynthetic processes that consumes dissolved inorganic carbon during primary production (Figure 4.4).

South of 42 ˚S (Southern zone, 42.2 – 45˚S), temperature and salinity decreased from 14.8 to 7 ˚C and from 34.76 to 33.48 due to the sub-Antarctic surface waters interleaving with surface waters associated with the Agulhas Return Current. The variability in temperature caused an increase in dissolved inorganic carbon from 2020 to 2070 $\mu mol.kg^{-1}$ and $dfCO_2$ gradient decreased from -40 to -15 µatm (Figure 4.4). Moreover, the freshening of sub-Antarctic waters also caused total alkalinity to decrease by 50 $\mu mol.kg^{-1}$ (from 2300 to 2250 $\mu mol.kg^{-1}$).
Total alkalinity decreased from 2300 to 2242 $\mu mol.kg^{-1}$ between 42.2 – 43 °S (Figure 4.4), the decrease was also a result of cooler and fresher sub-Antarctic surface waters interleaving with surface waters associated with the Agulhas Return Current. Temperature and dissolved inorganic carbon decreased from 15 to 11 °C and from 2060 to 2020 $\mu mol.kg^{-1}$, and chlorophyll-a concentration increased from 0.3 to 0.8 $mg.m^{-3}$, due to primary production processes that consumes dissolved inorganic carbon and nutrients to produce chlorophyll.

In order to determine the main mechanism (biological or the solubility pumps) responsible for CO_2 sink in the sub-Tropical and sub-Antarctic zones; the relationships between temperature and fCO_2 will be discussed in order to determine the effects of the solubility pump on carbon drawdown. Similarly, the relationship between fCO_2 and chlorophyll-a concentration will be discussed in order to determine the effects of the biological pump on carbon drawdown in these zones. Temperature and chlorophyll-a concentration are independent variables whilst fCO_2 is a dependent variable (i.e. changes in temperature and

chlorophyll-a concentration influences variability in fCO_2) when examining the effects of the solubility and biological pumps on carbon uptake.

The sub-Tropical zone had no correlation between temperature and fCO_2 due to the low R^2 (correlation coefficient) value of 0.0012 (Table 5.1). As a consequence, temperature variability was not responsible for CO_2 drawdown, thus the solubility pump played minimal role in the uptake of CO_2.

Similarly, the biological pump also played minimal role in CO_2 drawdown because there was no relationship (R^2=0.12) between fCO_2 and chlorophyll-a concentration, as a result of relatively low $dfCO_2$ gradient (-40 µatm) in the northern edge and the relatively high $dfCO_2$ gradient (-70 µatm) in the southern edge resulting in an offset of the effects of primary production on carbon drawdown. Furthermore, the increased $dfCO_2$ gradient in the southern edge was caused by the decline in total alkalinity that decreased dissolved inorganic carbon confirming that primary production did indeed occur. Similarly, primary production also occurred in the northern edge due to the relatively low dissolved inorganic carbon reduced during chlorophyll production.

Table 5.1: Regression table used to determine the mechanism responsible for CO_2 uptake in the sub-Tropical and sub-Antarctic zones along the Crossroads cruise track. Temperature (°C), chlorophyll-a concentration (Chl-a, mg.m^{-3}) and fugacity of carbon dioxide (fCO_2, µatm) will be used in determining whether the sink of CO_2 was a result of the biological or solubility pump. R^2 denotes the correlation coefficient and the equation is the regression line that can be used to calculate missing independent or dependent variables.

Zone	Dependent variable (y)	Independent variable (x)	Correlation coefficient (R^2)	Regression equation	Station
Sub-Tropical	fCO_2	Temperature	0.0012		12CTD, 19XBT
	fCO_2	Chl-a	0.12		
Sub-Antarctic	fCO_2	Temperature	0.50		6CTD, 15XBT
	fCO_2	Chl-a	0.0054		

An inverse fCO_2-temperature relationship was observed in the sub-Antarctic zone with a correlation coefficient of 0.5 (R^2=0.5) (Table 5.1), implying that temperature variability might have played a significant role in explaining changes in fCO_2 through the solubility pump. Additionally, R^2 value suggested that other processes such as biological processes might have been responsible for the remaining variability in fCO_2. The negative gradient confirmed by Sarmiento and Gruber (2006) statement about the inversely proportional relationship between dissolve inorganic carbon and temperature. Additionally, Takahashi et al (2002) stated that the surface fCO_2 is decreased by the cooling effect on warm waters and by the biological drawdown of fCO_2. On average high CO_2 flux was experienced in the sub-Antarctic

zone, as a result of the sub-Antarctic surface waters being ~6 °C cooler than the sub-Tropical surface waters (Table 4.3), causing an increase in CO_2 solubility coefficient thus reducing fCO_2 of the surface ocean, resulting in more carbon uptake by the ocean.

There was no relationship between chlorophyll-a concentration and fCO_2 in the sub-Antarctic zone as R^2 was 0.0054 (correlation coefficient) and had a negative regression gradient. As a result, the biological pump was not responsible for carbon drawdown implying that the solubility pump was largely responsible for changes in chlorophyll-a concentration. The increase in chlorophyll was a result of nutrients being brought up to the surface via upwelling processes thus enhancing primary production.

In summary, the solubility pump was also responsible for the carbon drawdown in the sub-Antarctic zone because the relationship between temperature and fCO_2 had a negative regression gradient at R^2 value of 0.5, and the sub-Antarctic zone was 0.6 °C cooler than the sub-Tropical zone (Table 5.1 and Table 4.3).
The biological pump was not responsible for carbon drawdown in the sub-Tropical zone because the biological effects that resulted in relatively low dissolved inorganic carbon in the northern region of the sub-Tropical zone and relatively high dissolved inorganic carbon in the southern region countered each other resulting in little to no effects on carbon drawdown. Moreover, the solubility pump also had little to no effect on carbon drawdown because there was no correlation between fCO_2 and temperature (Table 5.1 and Table 4.3).

5.2 What are the differences between the three regimes (Agulhas Current, Inner Retroflection Loop and Agulhas Return Current) of the Agulhas Current system?

The Agulhas Current system consists of three regimes; the Agulhas Current, the Inner retroflection Loop (IRL) and the Agulhas Return Current regions found in the sub-Tropical zone.

The lowest dissolved inorganic carbon in the Agulhas Current region was seen at ~36.6 ˚S due to the 0.5 ˚C (21.5 to 22 ˚C) increase in temperature due to the presence of the Agulhas Front promoting mixing of warm Agulhas Current surface waters with its ambient waters (Figure 4.5). Dissolved inorganic carbon decreased from 2028 to 2020 μmol.kg^{-1} thus decreasing dfCO_2 gradient by -10 μmol.kg^{-1} (from -50 to -40 μmol.kg^{-1}) (Figure 4.5).

The Inner Retroflection Loop (IRL) is a region of large exchange of heat and salt between the Indian and Atlantic Oceans, this is the area where the Agulhas Rings are formed and ejected into the Atlantic Ocean. The IRL had the lowest mean temperature value of 20.68 ˚C (Table 4.2) and resulted in the highest mean dissolved inorganic carbon of 2331.1 μmol.kg^{-1} (Figure 4.5), this was a consequence of the inverse relationship between dissolved inorganic carbon and temperature. Moreover, the low chlorophyll-a concentration suggested that the region lacked nutrients that would have been used together with dissolved inorganic carbon during photosynthetic processes that would have increased chlorophyll-a concentration.

The lowest mean dissolved inorganic carbon of the Agulhas Current system was observed in the Agulhas Return Current region at a value of 2013 μmol.kg^{-1} (Figure 4.5). Total alkalinity also decreased to a minimum value of 2327 μmol.kg^{-1} causing a 16 μmol.kg^{-1} (from -49 to -65 μmol.kg^{-1}) increase in dfCO_2 gradient resulting in maximum chlorophyll-a concentration of 0.45 mg.m^{-3} (Figure 4.5). Additionally, primary production was responsible for the relatively low dissolved inorganic carbon and the relatively high chlorophyll concentration.

5.3 What mechanisms account for the changes within the Agulhas Current system?

In order to determine whether the solubility pump was responsible for CO_2 sink, the relationship between temperature and fCO_2 will be discussed. Additionally, temperature and chlorophyll-a concentration are independent variables whilst fCO_2 is a dependent variable. Determining whether the biological pump was responsible for carbon uptake, the relationship between fCO_2 and chlorophyll-a concentration will be examined.

The opposing effect between chlorophyll and temperature on pCO_2 explains why although there is carbon drawdown by primary production in the Agulhas and Agulhas Return Current regions, this is not reflected in the pCO_2 as illustrated by the very low correlation coefficients (Table 5.2). The possible correlation between pCO_2 and chlorophyll-a concentration was offset by the warming in the Agulhas and Agulhas Return Currents regionally which reduced the solubility of CO_2 and increases the pCO_2 thus breaking down the initial chlorophyll-pCO_2 correlation.

This is important because it means that although the Agulhas and Agulhas Return Currents may be sinks of carbon, this does not play a role in enhancing the air – sea exchange of CO_2.

Table 5.2: Regression table used to determine the mechanism responsible for CO_2 uptake in the Agulhas Current, Inner Retroflection Loop (IRL) and Agulhas Return Current regions along the Crossroads cruise track. Temperature (°C), chlorophyll-a concentration (Chl-a, mg.m^{-3}) and fugacity of carbon dioxide (fCO_2, µatm) will be used in determining whether the sink of CO_2 was a result of the biological or solubility pump. R^2 denotes the correlation coefficient and the equation is the regression line that can be used to calculate missing independent or dependent variables.

Region	Dependent variable (y)	Independent variable (x)	Correlation coefficient(R^2)	Regression equation
Agulhas Current	fCO_2	Temperature	0.28	
	fCO_2	Chl-a	0.0077	
IRL	fCO_2	Temperature	0.022	
	fCO_2	Chl-a	0.017	
Agulhas Return Current	fCO_2	Temperature	0.21	
	fCO_2	Chl-a	0.51	

Summary of Chapter 5.1 – 5.3

The sub-Tropical zone was warm and saline whilst the sub-Antarctic zone was cool and fresh (Figure 4.4). The Agulhas Current system is located within the sub-Tropical zone between 36.5 – 38.5 ˚S, thus both the Agulhas Current system and the sub-Tropical zone are oligotrophic resulting in maximum chlorophyll-a concentration of 0.5 mg.m^{-3}.

The sub-Tropical zone had no correlation between temperature and fCO_2 (Table 5.1), therefore temperature variability was not responsible for CO_2 drawdown confirming that the solubility pump played a minimal role on the uptake of CO_2. Similarly, the biological pump also played a minimal role on carbon drawdown in the sub-Tropical zone due to the offset of biological processes in the northern (Agulhas Current) and southern (Agulhas Return Current) zones of the subtropical zone. The northern region had relatively low dissolved inorganic carbon which resulted from relatively high chlorophyll-a concentration, meanwhile the southern region also had relatively high chlorophyll concentration at high dissolved inorganic carbon contents due to decreasing total alkalinity that increased fCO_2 towards the sub-Tropical Convergence.

Biological pump played no role on CO_2 air – sea gas exchange in the Agulhas Current region because the effects of temperature and dissolved inorganic carbon on fCO_2 cancelled each other out. For example, as fCO_2 increased due to primary production that resulted in increased chlorophyll concentration and decreased dissolved inorganic carbon. Similarly, temperature decreased south of 36.6 °S causing dissolved inorganic carbon to increase. The increase in dissolved inorganic carbon will decrease fCO_2 that will in turn increase chlorophyll-a concentration. Thus the decrease in dissolved inorganic carbon due to primary production and the decrease in dissolved inorganic carbon due to increasing temperature resulted in an offset of the effects of fCO_2 on chlorophyll in the Agulhas Current system.

The solubility pump played a major role in the drawdown of carbon in the sub-Antarctic zone, since the sub-Antarctic surface waters were ~6 °C cooler than the sub-Tropical surface waters (Table 4.3). Furthermore, decreasing total alkalinity caused an increase in fCO_2 that decreased dissolved inorganic carbon resulting in relatively high chlorophyll-a concentration. Hence, areas of high chlorophyll concentration had $dfCO_2$ values that were more positive, for example

at 38.5 °S chlorophyll-a concentration was 0.9 $mg.m^{-3}$ and $dfCO_2$ gradient was -19 $mmolC.m^{-2}day^{-1}$.

A remarkable observation was seen in the changes in CO_2, temperature and salinity directly south of the Agulhas Return Current (Figure 4.4). These changes were consistent with that of a mesoscale feature assumed to be of Agulhas Current origins. The question that remained was whether the mesoscale feature was an Agulhas Plateau eddy and if so, was it a regular feature across the Agulhas Plateau?

5.4 What are the biogeochemical characteristics of the Agulhas Plateau eddy?

A relatively warm (~17 ˚C) and salty (~35.5) mesoscale feature was observed in Figure 4.4, it had a diameter of ~301 km and a maximum sea surface height of ~60 cm, resulting in a positive sea surface signal consistent with that of a warm-core anticyclonic eddy found in the Southern Hemisphere (Figure 5.1). Furthermore, the diameter of the feature was consistent with that of an anticyclonic eddy studied by Boebel et al (2003) in September 1999.

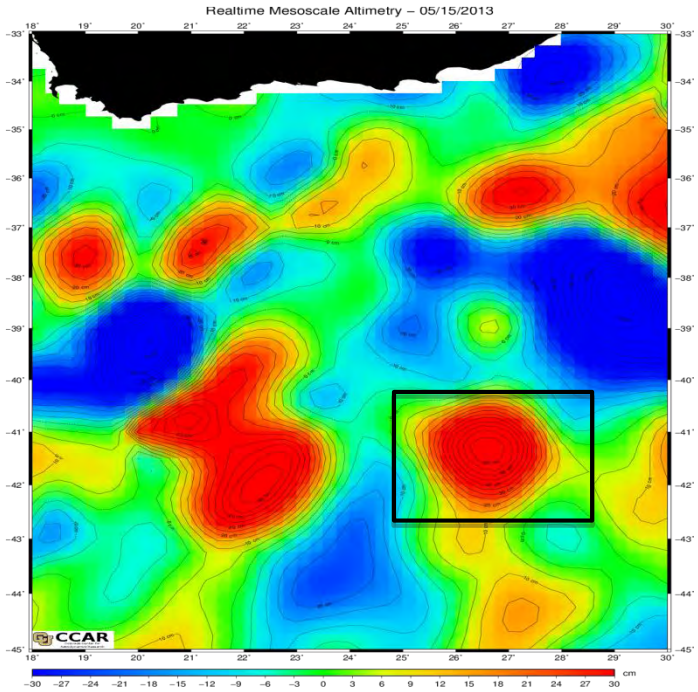

Figure 5.1: Satellite sea surface height plot, used to allocate the Agulhas Plateau eddy enclosed in the black square box. Satellite sea surface height is for the 15th May 2013 obtained from the Colorado Center for Astrodynamics Research (CCAR) website (http://eddy.colorado.edu/ccar/data_viewer/contact).

According to Boebel et al (2003), anticyclonic eddies are shed from the Agulhas Return Currents crest as it interacts with the Agulhas Plateau (bathymetric obstacle of 400 km meridional extent), but have a short lifespan due to either re-absorption or dissipation (Lutjeharms, 1988). Boebel et al (2003) further added that the maximum southerly extension of these eddies were ~42 ˚S, for the purpose of this study the anticyclonic eddy was referred to as the Agulhas Plateau eddy. The Agulhas Plateau eddy in Figure 5.2 was indeed a warm-core anticyclonic eddy, because it rotated from east to west with a maximum rotation speed of 1 $m.s^{-1}$ centred at 41 ˚S and its maximum sea surface temperature was 17 ˚C (Figure 4.2).

The positive sea surface signal was caused by the deepening of the thermocline that resulted in upwelling and downwelling dynamics in the edges and the core of the eddy, respectively

(Figure 5.2). In addition, Siegel et al (1999) confirmed that an anticyclonic feature (high sea level anomaly) will depress isopycnals out of the euphotic zone, transporting nutrient-depleted water downward. Therefore, higher primary production is expected on the edges of the eddy via Ekman transport forcing nutrients to the left in the Southern Hemisphere (McGillicuddy and Robinson, 1997).

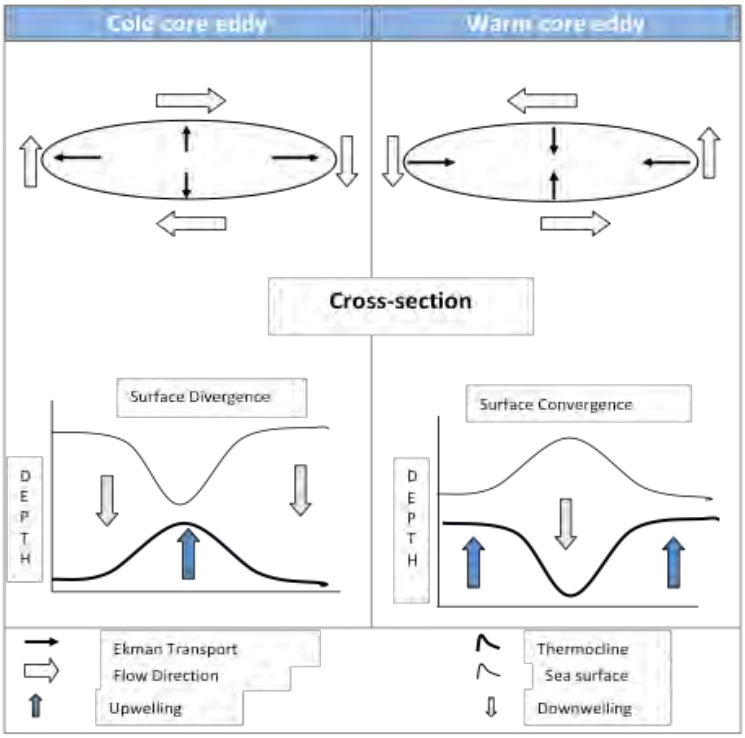

Figure 5.2: A conceptual model of the physical representation of warm and cold core eddies in the Southern Hemisphere.

The Agulhas Plateau eddy interleaves both Sub-Tropical and Sub-Antarctic water masses between 40 – 42 ˚S. Its location brings about alterations in temperature; salinity, chlorophyll-a, dissolved inorganic carbon and total alkalinity (Figure 4.4).

The temperature and salinity of the Agulhas Plateau eddy ranged between 13 - 17.5 ˚C and 35 – 35.6 consistent with Agulhas water masses (Lutjeharms and Ansorge, 2001; Figure 4.4). The average temperature and salinity values are 16.54 ˚C and 35.3 (Figure 4.4). Furthermore, dissolved inorganic carbon; total alkalinity and chlorophyll-a concentration ranged between 2060 – 2070 µmol.kg^{-1}, 2320 – 2340 µmol.kg^{-1} and 0.28 – 0.4 mg.m^{-3} respectively. The mean dissolved inorganic carbon, total alkalinity and chlorophyll-a concentrations were 2060 µmol.kg^{-1}, 2330 µmol.kg^{-1} and 0.34 mg.m^{-3}.

A positive-linear relationship (R^2=0.76) between fCO_2 and temperature in the eddy was experienced (Table 5.3). According to Chen et al (2007), a positive-linear relationship in an anticyclonic eddy suggests that downwelling is the primary mechanism responsible for variability in fCO_2. As previously stated downwelling occurred in the centre of the eddy, allowing more atmospheric carbon uptake in the centre than the edges. Therefore, dissolved inorganic carbon increases in the centre (Figure 4.4).

Table 5.3: Regression table used to determine the mechanism responsible for CO_2 uptake in the Agulhas Plateau eddy region along the Crossroads cruise track. Temperature (°C), chlorophyll-a concentration (Chl-a, mg.m^{-3}) and fugacity of carbon dioxide (fCO_2, µatm) will be used in determining whether the sink of CO_2 was a result of the biological or solubility pump. R^2 denotes the correlation coefficient and the equation is the regression line that can be used to calculate missing independent or dependent variables.

Dependent variable (y)	Inependent variable (x)	Correlation coefficient (R^2)	Regression equation
fCO_2	Temperature	0.76	$y = 6.12x + 24564$
fCO_2	Chl-a	0.54	$y = -0.0062x + 2.35$

Upwelling and downwelling processes caused an increase in chlorophyll-a concentration on its edges and a decrease in concentration on its centre. A negative relationship between chlorophyll-a concentration and fCO_2 was observed with a R^2 value of 0.54 (Table 5.3). The negative relationship infers that as chlorophyll-a concentration increases as a result of photosynthesis, fCO_2 will automatically decreases due to the increasing dissolved inorganic carbon brought about by upwelling processes on the edges of the eddy.

The Agulhas Plateau eddy was on average ~ 4 °C cooler than the Agulhas Return Current (Table 4.3). As a consequence, cooler surface waters in the eddy region increased the solubility of CO_2 that in term increased CO_2 flux by a magnitude of 1.82 mmolC.m^{-2}.day^{-1} (from -6.30 to -8.12 mmolC.m^{-2}.day^{-1}). Moreover, the average wind speed in the Agulhas Plateau eddy region was 3 m.s^{-1} greater than the wind speed in the Agulhas Return Current (Table 4.3), thus higher wind speeds also increase carbon uptake via bubbling and mixing etc.

In summary, temperature variability and biological processes were responsible for carbon drawdown, therefore the solubility and biological pumps were responsible for CO_2 air – sea gas exchange in the Agulhas Plateau eddy. The question remains; is the Agulhas Plateau eddy observed in May 2013 a regular feature over the plateau?

5.5 Is the eddy a regular feature? 2012 and 2013 datasets were used to answer this question.

The temperature profile for both (2012 and 2013) datasets followed the same trend (i.e. temperature decreasing as currents moves south away from the Agulhas Current region) (Figure 5.3). Temperature for 2012 was warmer by ~2.5 °C than 2013, but it must be noted that the two transects were not entirely identical.

Both underway transects showed a rapid increase in temperature and salinity profiles (~2.5 °C and salinity ~1.5) between 40 and 44 °S, resulting in a warmer and saltier body of water displaced across the Agulhas Plateau (Figure 5.3). The increase in temperature and salinity between 40 and 42 °S for the year 2013, clearly showed that the feature consist of Agulhas Current properties (Figure 4.4) and the current flow of the feature confirmed that eddy was indeed an anticyclonic Agulhas Plateau eddy confined across the Agulhas Plateau (Figure 5.1). Similarly, the increase of both temperature and salinity for 2012 between 42 and 44 °S also confirm the presence of an anticyclonic Agulhas Plateau eddy (Figure 5.3).

As mentioned earlier in this section, transects for both years were not identical and the eddy observed in Figure 5.3 for 2012 could not be compared to that of 2013. Consequently, physical dynamics (such as, upwelling and downwelling activities) for 2012 eddy could not be identified with accuracy. Thus due to lack of pCO_2 underway data the regularity of the Agulhas Plateau eddy could not be answered, instead satellite sea surface height imagery was obtained from the CCAR website for 2012 and 2013 during the month of May to answer the question: Is an Agulhas Plateau eddy a regular feature?

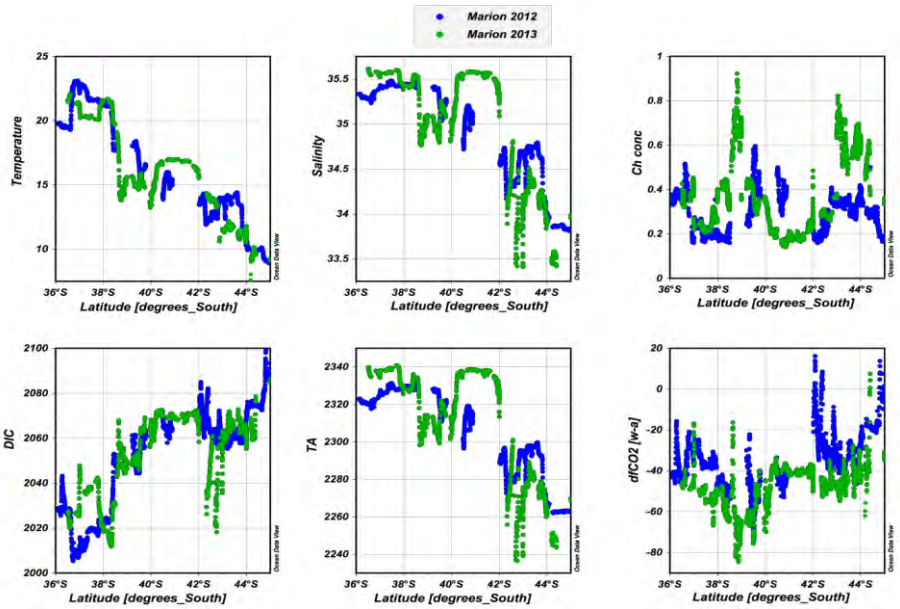

Figure 5.3: Surface property plots of the cruise tracks from Cape Town to Marion Island for the years 2012 and 2013, demonstrating temperature in ^{0}C (a), salinity in psu (b), chlorophyll-a concentration (Ch conc) in $mg.m^{-3}$ (c), DIC (dissolved inorganic carbon) (d), TA (total alkalinity) (e) and $dfCO_2$ [w-a](exchange of CO_2 between the ocean and the atmosphere, in µatm) (f). Total alkalinity and dissolved inorganic carbon both measured in $umol.kg^{-1}$. Positive $dfCO_2$ [w-a] values (>0 µatm) indicate CO_2 outgassing by the ocean and negative values (<0 µatm) CO_2 ingassing.

Sea surface height (Figure 5.4a) imagery for 2012 showed a warm-core anticyclonic eddy across longitudinal range of 22 – 26 ˚E with a width of ~301 km and a sea surface height of 70 cm. Similarly, a warm-core anticyclonic eddy was also observed in Figure 5.4.2b with a sea surface height of 60 cm, a width of ~501 km and a longitudinal range between 25 – 28 ˚E. In addition, eddies from both years were located between 40 – 43 ˚S. Therefore, the Agulhas Plateau eddy observed in both sea surface height imageries for 2012 and 2013 confirmed that the Agulhas Plateau eddy was a regular feature and should be expected to be seen throughout future Crossroads cruise line (Figure 5.4).

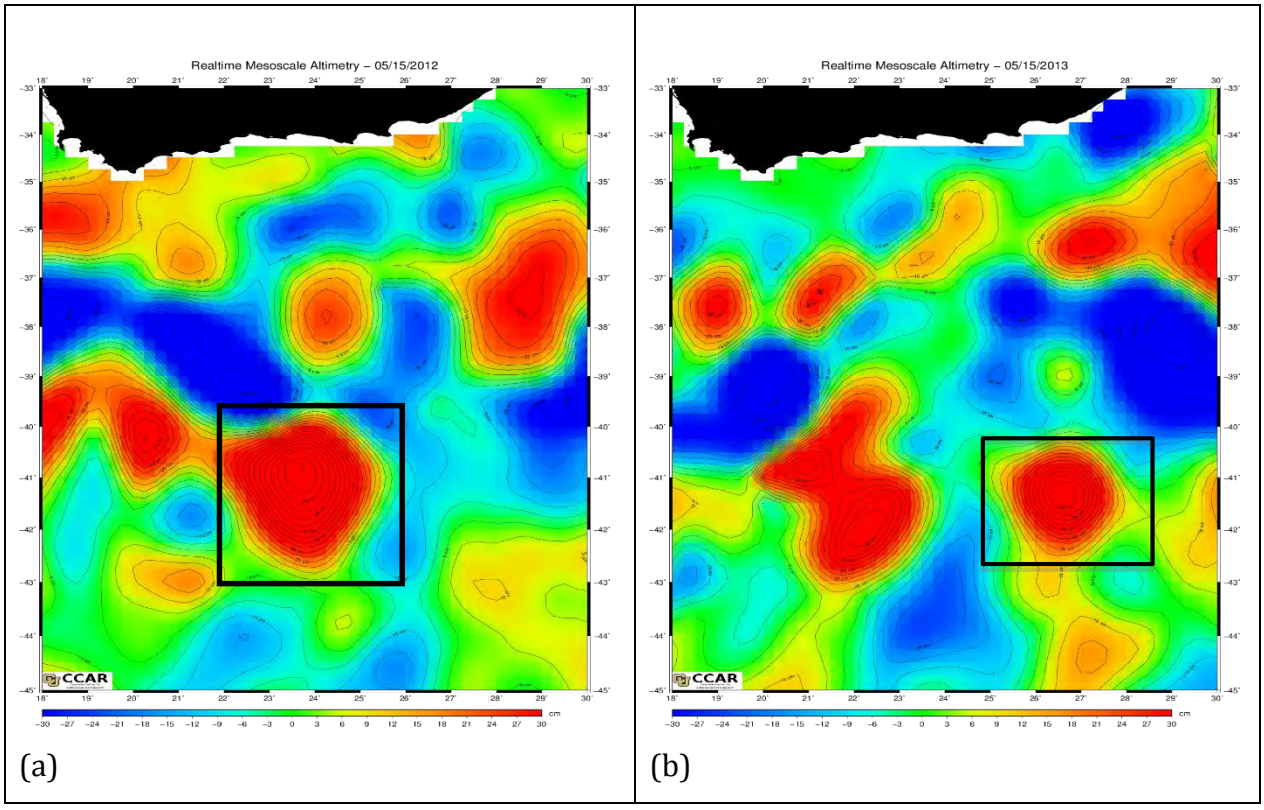

Figure 5.4: Satellite sea surface height (SSH) plot, (a) for 2012 and (b) for 2013. The SSH plot is used to allocate the Agulhas Plateau eddy enclosed in the black square box. Satellite sea surface height is for the 15th May 2013 obtained from the Colorado Center for Astrodynamics Research (CCAR) website (http://eddy.colorado.edu/ccar/data_viewer/contact).

6. Conclusion

In-situ measurements collected along the entire Crossroads transect augmented with remote-sensing data were analyzed to establish the role of the Agulhas Current system (Agulhas and the Agulhas Return Currents) in the uptake of CO_2 and to identify the main mechanism responsible for this influx. The Crossroads transect presents an unique opportunity to establish the role Western Boundary Currents (WBCs) of the Southern Hemisphere have on CO_2 influx and how this region compared with the cooler sub-Antarctic environment to the south.

The first objective of this study was investigated in Chapter 4, which highlighted the differences between CO_2 characteristics in the sub-Tropical zone, sub-Antarctic zone, Agulhas and Agulhas Return Currents.

The sub-Tropical zone consists of the Agulhas Current system (Agulhas and the Agulhas Return Currents), hence the region was warm-saline and oligotrophic. Furthermore, the region had maximum chlorophyll-a concentration of 0.4 $mg.m^{-3}$ related with the sub-Tropical gyre. The sub-Antarctic zone was divided into two parts due to the presence of the Agulhas Plateau eddy; the Northern (38.6 – 39.8 ˚S, the region north of the Agulhas Plateau) zone experienced a 5 ˚C drop in temperature that resulted in an increased dissolved inorganic carbon due to the transition from warm-saline Agulhas Current surface waters to cool-less saline sub-Antarctic surface waters and Southern (42.2 – 45 ˚S, region after the Agulhas Plateau eddy) zone, experienced temperature decrease and $dfCO_2$ gradient increased resulting in relatively more carbon uptake and chlorophyll-a concentration compared to the Northern zone (Table 4.1).

The second objective was aimed at examining the main mechanism (solubility or biological pump) responsible for oceanic CO_2 uptake in these regions (sub-Tropical region, sub-Antarctic region and Agulhas Current system) and how they differed from one another?
The solubility pump was responsible for carbon uptake in the sub-Antarctic zone but neither pumps were responsible for carbon uptake in the sub-Tropical zone.
The solubility and biological pumps had minimal to no effect on carbon drawdown in the Agulhas and Agulhas Return Current regions. Carbon sink in the Agulhas Current system was due to the opposing effect between chlorophyll and temperature on pCO_2, this explains why although there is carbon drawdown by primary production in the Agulhas and Agulhas Return Current regions, this is not reflected in the pCO_2 as seen by the very low correlation coefficients (Table 5.2). The possible correlation between pCO_2 and chlorophyll-a concentration was offset by the warming in the Agulhas and Agulhas Return Currents regionally which reduces the solubility of CO_2 and increases the pCO_2 thus breaking down the initial chlorophyll-pCO_2 correlation.
This is important because it means that although the Agulhas and Agulhas Return Currents may be sinks of carbon, this does not play a role in enhancing the air – sea exchange of CO_2.

A mesoscale feature, possibly representing an Agulhas eddy was seen directly south of the Agulhas Return Current over the Agulhas Plateau (Figure 5.1). The mesoscale feature brought about the fourth and fifth questions that were also answered in Chapter 5; the question was to determine whether the mesoscale feature assumed to be of Agulhas Current origins was indeed an Agulhas Plateau eddy and whether the mesoscale feature was a regular feature?
The mesoscale feature was indeed of Agulhas Current origins as it had mean temperature value of 16.54 ˚C and a mean salinity value of 35.25 (Figure 4.4), and was located over the Agulhas Plateau; for this study the eddy was then referred to as the Agulhas Plateau eddy. It was also proven that temperature variability was the main driver behind CO_2 sink confirming

that the solubility pump was the main mechanism responsible for carbon drawdown within the Agulhas Plateau eddy. The Agulhas Plateau is an area of high mesoscale variability with sea surface height for 2009 - 2013 (Figure 6.1) showing an eddy to be present over the plateau on average 63% of the time (Figure 5.4). The eddy region (40 – 42 ˚S) was a stronger sink of CO_2 than the Agulhas and the Agulhas Return Currents due to the high mean wind speed (12.23 $m.s^{-1}$) and lowest mean temperature (16.54 ˚C) (Table 4.2), resulting in more CO_2 influx in the Agulhas Plateau eddy.

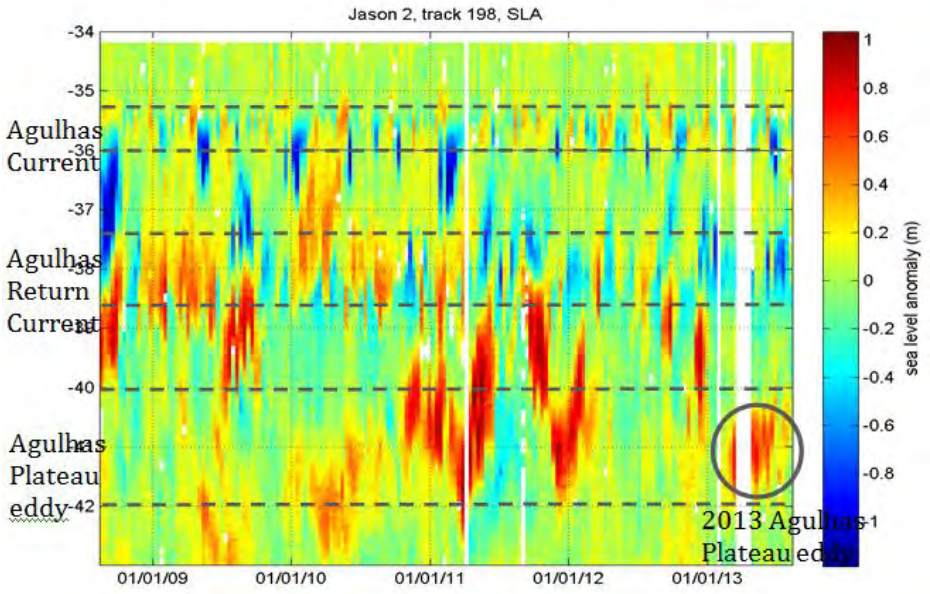

Figure 6.1: A Hofmuller plot for the period 2009-2013 along the Crossroads altimetry line highlighting the location of positive anomalies associated with warm eddies over the Agulhas Plateau (adapted from J. Book).

Mid-high latitude in the southern ocean constitutes a sink of -1.05 $PgCy^{-1}$. The climatological mean annual air-sea CO_2 flux for the reference year 2000 for the Agulhas and the Agulhas

Return Currents is ~-24 $gC.m^{-2}.year^{-1}$ (Takahashi et al, 2009), and for this study the annual mean of CO_2 flux based merely on April 2013 dataset was -10.37 $gC.m^{-2}.year^{-1}$.

This work offers new findings, but clearly calls for a more comprehensive analysis of the oceanic CO_2 sink in the Agulhas Current system. Long-term *in-situ* measurements of CO_2 at depth are necessary if the role the Agulhas Current system plays on the global carbon budget is to be better understood. More importantly with a changing climate and observations of a warming Agulhas Current (Rouault et al, 2009), what effects will this have on the CO_2 balance of this region?

7. Reference

- Andersson A.J, Krug L.A, Bates N.R and S.C Doney. (2013). Sea–air CO_2 flux in the North Atlantic Subtropical gyre: Role and influence of sub-Tropical Mode Water formation. *Deep Sea Research* , 57–70.
- Andres R.J, Fielding D.J, Marland G, Boden T.A and N Kumar. (1999). Carbon dioxide emissions from fossil-fuel use, 1751-1950. *Tellus* , 759-765.
- Ansorge I.J and J.R.E Lutjeharms. (2007). The Cetacean Environment off Southern Africa. pp 1-13. In: Whales and Dolphins of the Southern African subregion Eds: P.Best and P.A.Folkens Cambridge University Press.
- Atkinson L.P. (2010). Chapter 3.1. Western boundary current overview. In: Liu K-K, Atkinson L, Quiñones R, Talaue-McManus L (ed) Carbon and Nutrient Fluxes in Continental Margins: A Global Synthesis. Berlin: IGBP Book Series Springer.
- Beal L and A Biastoch. (2010). Improving Understanding of the Agulhas Current and Its Global Climate Impacts. *Eos, Transactions American Geophysical Union 91.*
- Beal L.M, De Ruijter W.P.M, Biastoch A, Zahn R and SCOR/WCRP/IAPSO Working Group 136. (2011). On the role of the Agulhas system in ocean circulation and climate . *Nature* , 429–436.
- Belkin I.M and A.L Gordon. (1996). Southern Ocean fronts from the Greenwich meridian to Tasmania. *Journal of Geophysical Research* , 3675-3696.
- Biastoch A, Boning C.W and J.R.E Lutjeharms. (2008). Agulhas leakage dynamics affects decadal variability in Atlantic overturning circulation. *Nature* , 489–492.
- Boutin J, Etcheto J, Merlivat L and Y Rangama. (2002). Influence of gas exchange coefficient parameterisation on seasonal and regional variability of CO_2 air-sea fluxes, *Geophysical Research Letter*, 1182.

- Brewer P.G, Wong G.T.F, Bacon M.P and D.W Spencer. (1975). An oceanic calcium problem? Earth Planet . *Science Letter* , 81-87.
- Brewer P.G and J Goldman. (1976). Alkalinity changes generated by phytoplankton growth. *Limnology Oceanography* , 108-117.
- Broecker W.S and T.H Peng. (1982). *Tracers in the sea.* Palisades, NY: Eldigeo Press.Lamont–Doherty Geological Observatory.
- Broecker W.S. (1991). The Great Ocean Conveyor. *Journal of Oceanography* , 79-89.
- Bryden H.L, Beal L.M and L.M Duncan. (2005). The structure and transport of the Agulhas Current and its temporal variability. *Journal of Oceanography* , 479-492.
- Caldeira K and M.E Wickett. (2003). Anthropogenic carbon and ocean pH. *Nature* , 365–365.
- Canadell J.G, Le Que´re´ C, Raupach M.R, Field C.B, Buitehuis E.T, Ciais P, Conway T.J, Gillett N.P, Houghton R.A and G Marland. (2007). Contributions to accelerating atmospheric CO_2 growth from economic activity, carbon intensity, and efficiency of natural sink. *Proceedings of the Natural Academy of Science* .
- Casal T.G.D, Beal L.M, Lumpkin R and W.E Johns. (2009). Structure and downstream evolution of the Agulhas Current system during a quasi-synoptic survey in February–March 2003. *Journal of Geophysical Research* .
- Cheney R.E, Marsh J.G and B.D Beckley. (1983). Global mesoscale variability from colinear tracks of SEASAT altimeter data. *Journal of Geophysical Research* , 4343-4354.
- Cronin M.F, Bond N, Booth J, Ichikawa H, Joyce T.M, Kelly K, Kubota M, Qiu B, Reason C, Rouault M, Sabine C, Saino T, Small J, Suga T, Talley L.D, Thompson L and R.A Weller. (2010). Monitoring ocean-atmosphere interactions in western boundary current extensions. In Proceedings of the "OceanObs'09: Sustained Ocean Observations and Information for Society" Conference (Vol. 2). Venice, Italy, 21-25 September 2009, Hall J, Harrison D.E and D Stammer D. Eds., ESA Publication WPP-306.

- Darbyshire J. (1972). The effect of bottom topography on the Agulhas Current. *Pure and Applied Geophysics* , 208-220.
- Dickson A.G and C. Goyet . (1994). *Handbook of methods for the analysis of the various parameters of the carbon dioxide system in sea water.* Washington, D.C: U.S. Dep. of Energy.
- Dickson A.G and F.J Millero. (1987). A comparison of the equilibrium constants for the dissociation of carbonic acid in seawater media. *Deep Sea Research* , 1733–1743.
- Dyrssen and L.G Sillén. (1967). Alkalinity and total carbonate in sea water. A plea for p-T independent data. http://onlinelibrary.wiley.com.ezproxy.uct.ac.za/doi/10.1111/j.2153-3490.1967.tb01464.x/pdf .
- Gille S.T. (2014). Meridional Displacement of the Antarctic Circumpolar Current, Philosiphical Transactions Royal Society A. 372. http://dx.doi.org/10.1098/rsta.2013.0273. (pdf, web,preprint)
- Gordon A.L. (1986). Interocean exchange of thermocline water. *Journal of Geophysical Research* , 5037–5046.
- Gordon A.L, Lutjeharms J.R.E and M.L Grüindlingh. (1987). Stratification and circulation at the Agulhas Retroflection. *Deep Sea Research* , 565-599.
- Gordon A.L, Lutjeharms J.R.E and M.L Grundlingh. (1987). Stratification and circulation at the Agulhas Retroflection. *Deep Sea Research* , 565–599.
- Grüindlingh M. (1983). On the course of the Agulhas Current. *South African Geography Journal* , 49-57.
- Heinze C, Maier-Reimer E and K Winn. (1991). Glacial pCO_2 reduction by the World Ocean: Experiments with the Hamburg Carbon Cycle Model. *Paleoceanography* , 395–430.
- Hoffman E. (1985). The large-scale horizontal structure of the Antarctic Circumpolar Current from FGGE drifters. *Journal of Geophysical Research* , 245-270.

- Huthnance J.M. (2010). The Northeast Atlantic margins, in Carbon and Nutrient Fluxes in Continental Margins: A Global Synthesis, edited by K.-K. Liu et al. *Springer*, *Berlin*. Section 5.2. 215-234.
- Iglesias-Rodriguez, M. & Co-Authors. (2010). Developing a Global Ocean Acidification Observation Network in these proceedings. *OceanObs09* , 24.
- IPCC. (2001). Climate change 2001: the scientific basis. In: Houghton, J.T., Ding Y, Griggs D.J, Noguer M, van der Linden P.J, Dai X, Maskell K and C.A Johnson. *Contribution of Working Group I to the Third Assessment Report of the Intergovernmental* .
- IPCC. (2007). Climate change 2007: the physical science basis. In: Solomon S, Quin D, Manning M, Chen Z, Marquis M, Averyt K.B, Tignor M, Miller H.L (Eds.). *Contribution of Working Group I of the Fourth Assessment Report of the Intergovernmental Panel on Cambridge University Press, Cambridge* , 996.
- Josey S.A, Kent E.C and P.K Taylor. (1999). New insights into the ocean heat budget closure problem from analysis of the SOC air-sea flux climatology. *Journal of Climate* , 2856–2880.
- Kondo J. (1976). Heat balance of the East China Sea during the Air Mass Transformation Experiment. *Journal of Meteorological Society of Japan* , 382–398.
- Kuhlbrodt T, Griesel A, Montoya M, Levermann A, Hofmann M and S Rahmstorf. (2007). On the driving processes of the Atlantic meridional overturning circulation. *Reviews of Geophysics (in press)* .
- Le Quéré C, Raupach M.R, Canadell J.G and G Marland et al. (2009). Trends in the sources and sinks of carbon dioxide. *doi: 10.1038/ngeo689* .
- Lee K, Tong L.T, Millero F.J, Sabine C.L, Dickson A.G, Goyet C, Park G.-H, Wanninkhof R, Feely R.A and R.M Key. (2006). Global relationships of total alkalinity with salinity and temperature in surface waters of the world's oceans. *Geophysical Research Letter* .
- Lewis E and D.W.R Wallace. (1998). *CO2SYS-Program developed for the CO_2 system calculations.* Carbon Dioxide Information and Analysis Centre.

- Lutjeharms J.R.E and H.R Valentine. (1984). Southern Ocean thermal fronts south of Africa . *Deep Sea Research* , 1461-1475.
- Lutjeharms J.R.E and I.J Ansorge. (2001). The Agulhas Return Current. Cape Town: Springer.
- Lutjeharms J.R.E, Bang N.D and C.P Duncan. (1981). Characteristics of the currents east and south of Madagascar. *Deep Sea Research* , 879-899.
- Lutjeharms J.R.E. (1988). Meridional heat transport across the Subtropical Convergence by a warm eddy. *Nature* , 251-254.
- Lutjeharms J.R.E. (2006). The Agulhas Current. *African Journal of Marine Science*, 729–730
- Lutjeharms, J.R.E and R.C van Ballegooyen. (1984). Topographic control in the Agulhas Current system. *Deep Sea Research* , 1321-1337.
- Mehrbach C, Culberson C.H, Hawley J.E and R.M Pytkowicz. (1973). Measurement of the apparent dissociation constants of carbonic acid in seawater at atmospheric pressure . *Limnology and Oceanography* , 897–907.
- Metzl N. (2009). Decadal increase of oceanic carbon dioxide in Southern Indian Ocean surface waters (1991–2007). *Deep Sea Research* , 607-619.
- Mey R.D and N.D Walker. (1990). Surface heat fluxes and marine boundary layer modification in the Agulhas retroflection region. *Journal of Geophysical Research* , 15997-16015.
- Millero F.J, Lee K and M Roche. (1998). Distribution of alkalinity in the surface waters of the major oceans. *Marine and Chemistry* , 111-130.
- Orsi A.H, Whitworth T and W.D Nowlin. (1995). On the meridional extent and fronts of the Antarctic Circumpolar Current. *Deep Sea Research* , 641–673.
- Park P.K. (1969). Oceanic CO_2 system: An evaluation of ten methods of investigation. *Limnology and Oceanography* , 179-186.

- Park Y.H, L Gamebroni and E Charriaud. (1991). Frontal structure and transport of the Antarctic Circumpolar Current in the south Indian Ocean sector, 40–80^0E. *Marine and Chemistry* , 45-62.
- Park Y.H, L Gamberoni and E Charriaud. (1993). Frontal structure, water masses and circulation in the Crozet Basin. *Journal of Geophysical Research* .
- Pérez F.F, Álvarez M and A.F Ríos. (2013). Improvements on the back-calculation technique for estimating anthropogenic CO_2. *Deep-Sea Research, submitted for publication* .
- Pierrot D, Neill C, Sullivan K, Castle R, Wanninkhof R, Lüger H, Johannessen T, Olsen A, Feely R.A and C.E Cosca. (2009). Recommendations for Autonomous Underway pCO_2 Measuring Systems and Data Reduction Routines. *Deep Sea Research* , 512-522.
- Raupach M.R, Marland G, Ciais P, Le Que´re´ C, Canadell J.G, Kleppe G and C.B Field. (2007). Global and regional drivers of accelerating CO_2 emissions. *Proceedings of the National Acadamy Sciences* , 10288–10293.
- Redfield A.C, Ketchum B.H and F.A Richards. (1963). The influence of organisms on the composition of seawater. *Journal of Geophysical Research* , 26-77.
- Riebesell U, Schulz K.G, Bellerby R.G.J, Botros M, Fritsche P, Meyerhofer M, Neill C, Nondal G, Oschlies A, Wohlers J and E Zollner. (2007). Enhanced biological carbon consumption in a high CO_2 ocean. *Nature* .
- Rintoul S.R. (1991). South Atlantic interbasin exchange. *Journal of Geophysical Research* , 2675–2692.
- Rouault M and J.R.E Lutjeharm. (2000). Air–sea exchanges over an Agulhas eddy at the Subtropical convergence. *Global Atmosphere–Ocean System* , 125–150.
- Rouault M, Reason C.J.C and J.R.E Lutjeharms. (2003). Underestimation of Latent and Sensible Heat Fluxes above the Agulhas Current in NCEP and ECMWF Analyses. *Journal of Climate* , 776–782.

- Rouault M, Penven P and B Pohl. (2009). Warming in the Agulhas Current system since the 1980's. *Geophysical Research Letter* .
- Sabine C.L, Feely R.A, Gruber N, Key R.M, Lee K, Bullister J.L, Wanninkhof R, Wong C.S, Wallace D.W.R, Tilbrook B, Millero F.J, Peng T.H, Kozyr A, Ono R, and A.F Rios. (2004). The oceanic sink for anthropogenic CO_2. *Science* , 367-371.
- Saetre R and A.J da Silva. (1984). The circulation of the Mozambique Channel. *Deep Sea Research* , 485-508.
- Sarmiento J.L and N Gruber. (2006). *Ocean Biogeochemical Dynamics.* Princeton and Oxford: Princeton University Press.
- Schlitzer R. (2009). *Ocean Data View.* Germany: Alfred Wegener Institute.
- Schmittner A, Chiang J.C.H and S.R Hemming. (2007). Introduction: The Ocean's Meridional Overturning Circulation. *American Geophysical Union* .
- Sigman D.M and E.A Boyle. (2000). Glacial/interglacial variations in atmospheric carbon dioxide. *Nature* , 859-869.
- Sigman D.M, Hain M.P and G.H Haug. (2010). The polar ocean and glacial cycles in atmospheric CO_2 concentration. *Nature* , 47 - 55
- Skirrow G. (1975). The dissolved gases—carbon dioxide. *Chemical Oceanography* , 1–192.
- Speich S, Blanke B, de Vries P, Drijfhout S, Doos K, Ganachaud A and R Marsh. (2002). Tasman leakage: A new route in the global ocean conveyor belt. *Geophysical Research Letter* .
- Stramma L, Ikeda Y and R.G Peterson. (1990). Geostrophic transport in the Brazil Current region north of 20 ˚S. *Deep Sea Research* , 1875-1886.
- Stumm W and J.J Morgan. (1981). Oceanic "C/'*C Observations: A new window on ocean CO_2 uptake. *Global Biogeochemical Cycles* , 353-368.
- Takahashi T et al. (2009). Climatological mean and decadal changes in surface ocean pCO_2, and net sea-air CO_2 flux over the global oceans. *Deep Sea Research* , 554–577.

- Takamitsu I and M.J Follows. (2003). Upper ocean control on the solubility pump of CO_2. *Journal of Marine Research* , 465–489.
- Thomalla S.J, Waldron H.N, Lucas M.I, Read J.F, Ansorge I.J and E. Pakhomov. (2011). Phytoplankton distribution and nitrogen dynamics in the southwest Indian subtropical gyre and Southern Ocean waters. *Ocean Science,* 113-127.
- van Sebille E, Beal L.M and A Biastoch. (2010). Sea surface slope as a proxy for Agulhas Current strength. *Journal of Geophysical Research* .
- Wanninkhof R and K Thoning. (1993). Measurement of fugacity of CO_2 in surface water using continuous and discrete sampling methods. *Marine and Chemistry* , 189-204.
- Weijer W, de Ruijter W.P.M and H.A Dijkstra. (2001). Stability of the Atlantic overturning circulation: Competition between Bering Strait freshwater flux and Agulhas heat and salt sources. *Journal of Physical Oceanography* , 2385–2402.
- Weiss R.F. (1974). Carbon dioxide in water and seawater: the solubility of a non-ideal gas. *Marine Chemistry* , 203–205.
- Wyrtki K. (1971). Oceanographic Atlas of the International Indian Ocean Expedition. *National Science Foundation* , 531.
- Xue H, Bane J.M and L.M Goodman. (1995). Modification of the Gulf Stream through strong air–sea interaction in winter: Observations and numerical simulations. *Journal of Physical Oceanography* , 533–557.
- Yu L. (2007). Global variations in oceanic evaporation (1958–2005): The role of the changing wind speed. *Journal of Climate* , 5376–5390.
- Zhang H.M, Reynolds R.W and J.J Bates. (2006). *Blended and Gridded High Resolution Global Sea Surface Wind Speed and Climatology from Multiple Satellites: 1987 - Present.* Atlanta, GA: American Meteorological Society 2006 Annual Meeting.